# Titanocene-gold complexes containing N-heterocyclic carbene ligands inhibit growth of prostate, renal and colon cancers *in vitro*

Yiu Fung Mui,[a,b#] Jacob Fernández-Gallardo,[a#] Benelita T. Elie,[a,c] Ahmed Gubran,[a] Irene Maluenda,[d] Mercedes Sanaú,[e] Oscar Navarro,[d] and María Contel*[a,b,c]

[a]Department of Chemistry, Brooklyn College, The City University of New York, Brooklyn, NY, 11210, US. [b]Chemistry and [c]Biology PhD Programs, The Graduate Center, The City University of New York, 365 Fifth Avenue, New York, NY, 10016, US. [d]Department of Chemistry, University of Sussex, Falmer, Brighton BN1 9QJ, U.K. [e]Departamento de Química Inorgánica, Universidad de Valencia, Burjassot, Valencia, 46100, Spain.

*Email: MariaContel@brooklyn.cuny.edu

**Supporting Information**

Table of Contents

**1.** NMR spectra of all compounds in $CDCl_3$

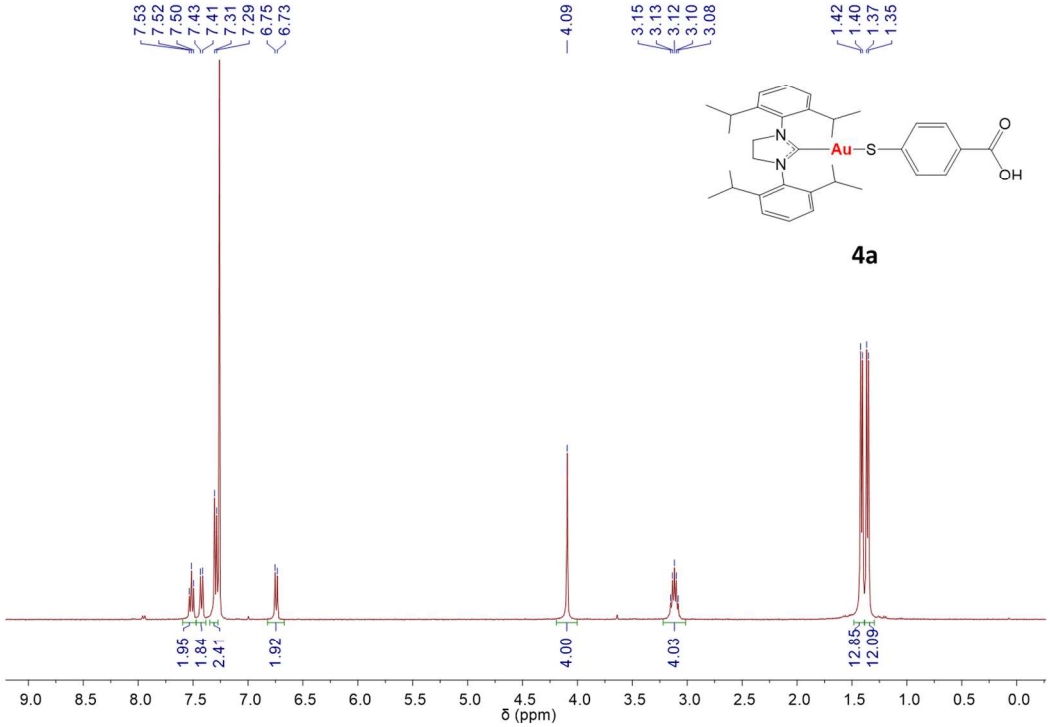


**Figure S1.** $^{1}H$ NMR spectrum of compound **4a** in $CDCl_3$.

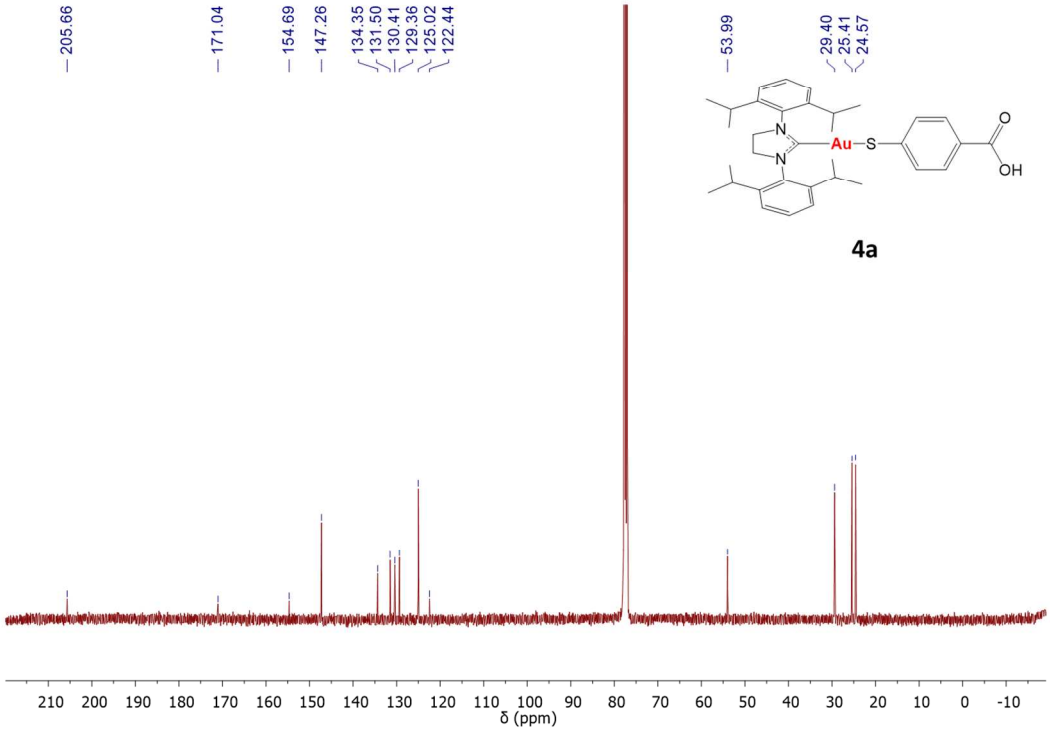


**Figure S2.** $^{13}C\{^{1}H\}$ NMR spectrum of compound **4a** in $CDCl_3$.

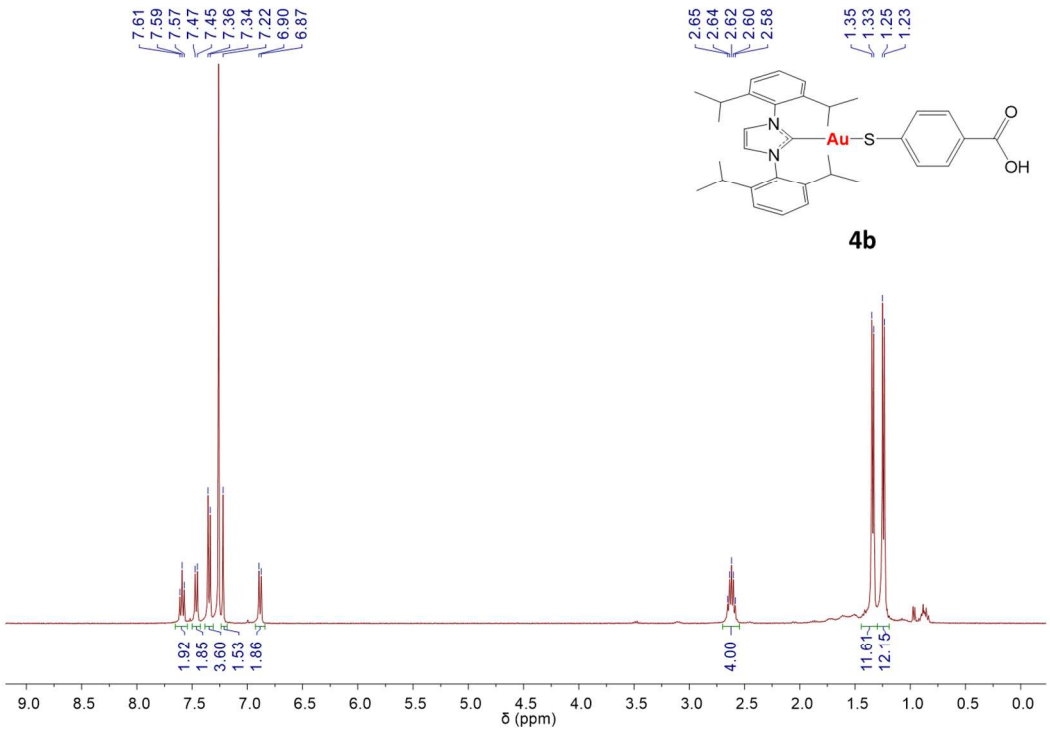


**Figure S3.** $^{1}H$ NMR spectrum of compound **4b** in $CDCl_3$.

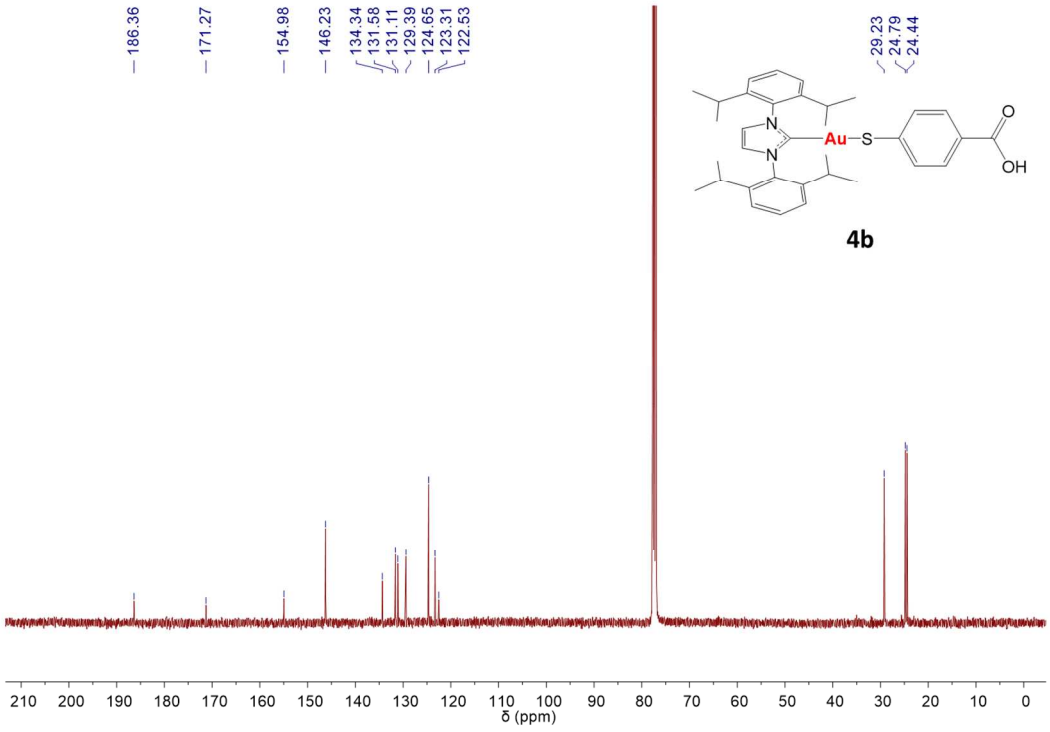


**Figure S4.** $^{13}C\{^{1}H\}$ NMR spectrum of compound **4b** in $CDCl_3$.

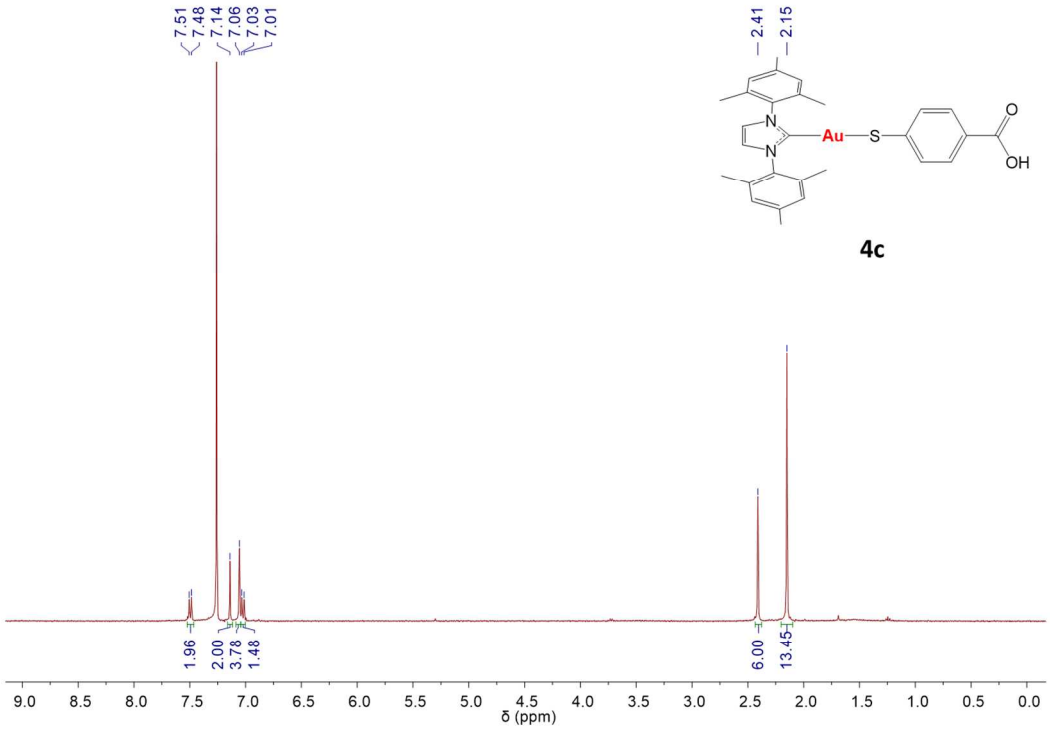


**Figure S5.** $^{1}H$ NMR spectrum of compound **4c** in $CDCl_3$.

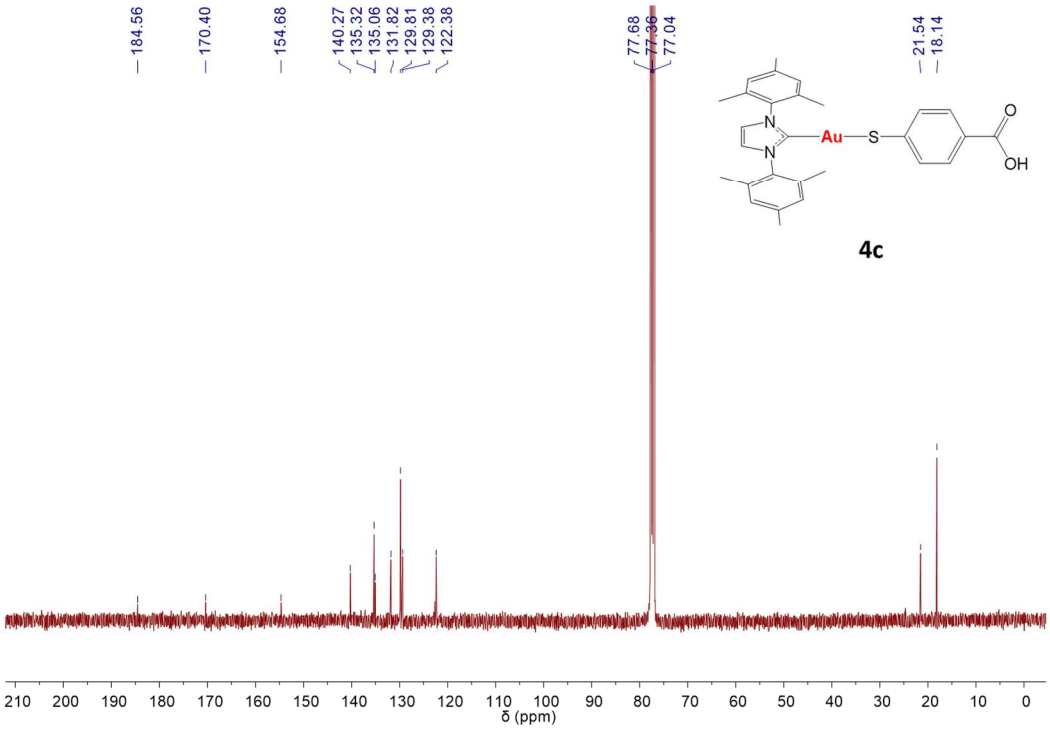


**Figure S6.** $^{13}C\{^{1}H\}$ NMR spectrum of compound **4c** in $CDCl_3$.

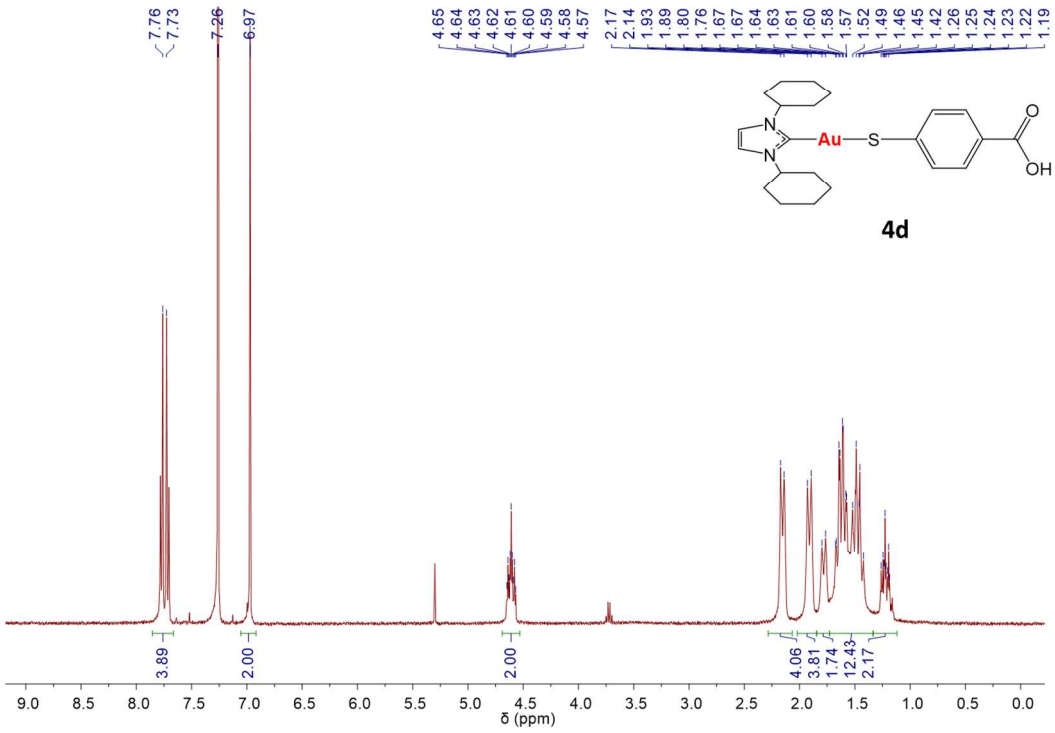


**Figure S7.** $^{1}H$ NMR spectrum of compound **4d** in $CDCl_3$.

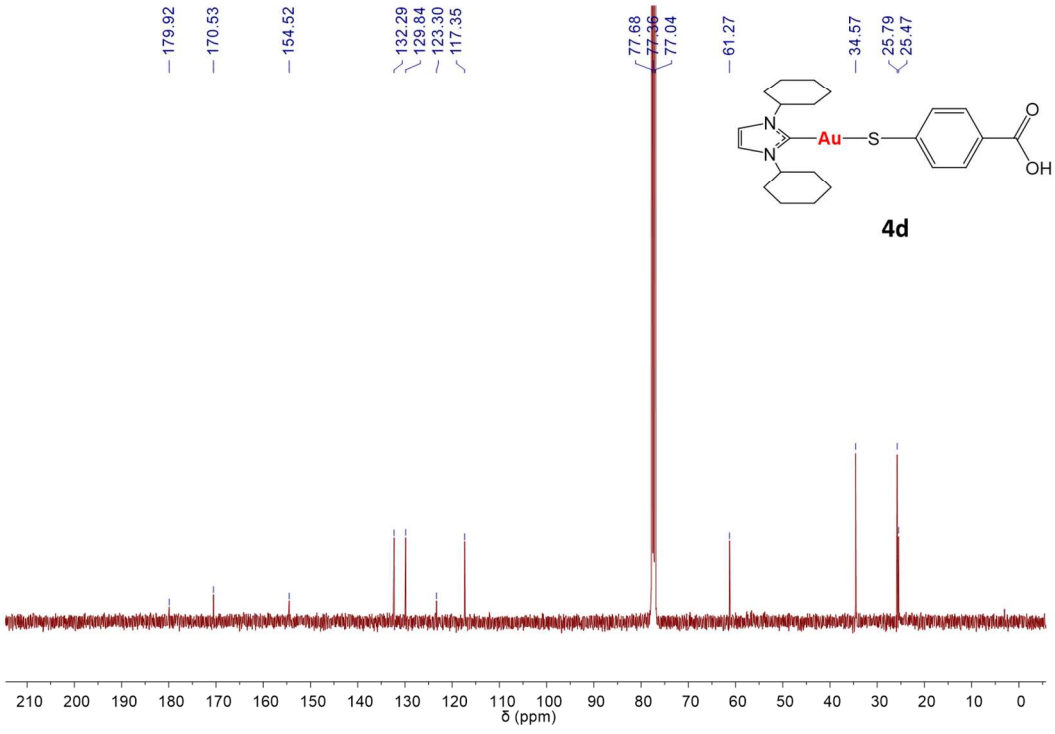


**Figure S8.** $^{13}C\{^{1}H\}$ NMR spectrum of compound **4d** in $CDCl_3$.

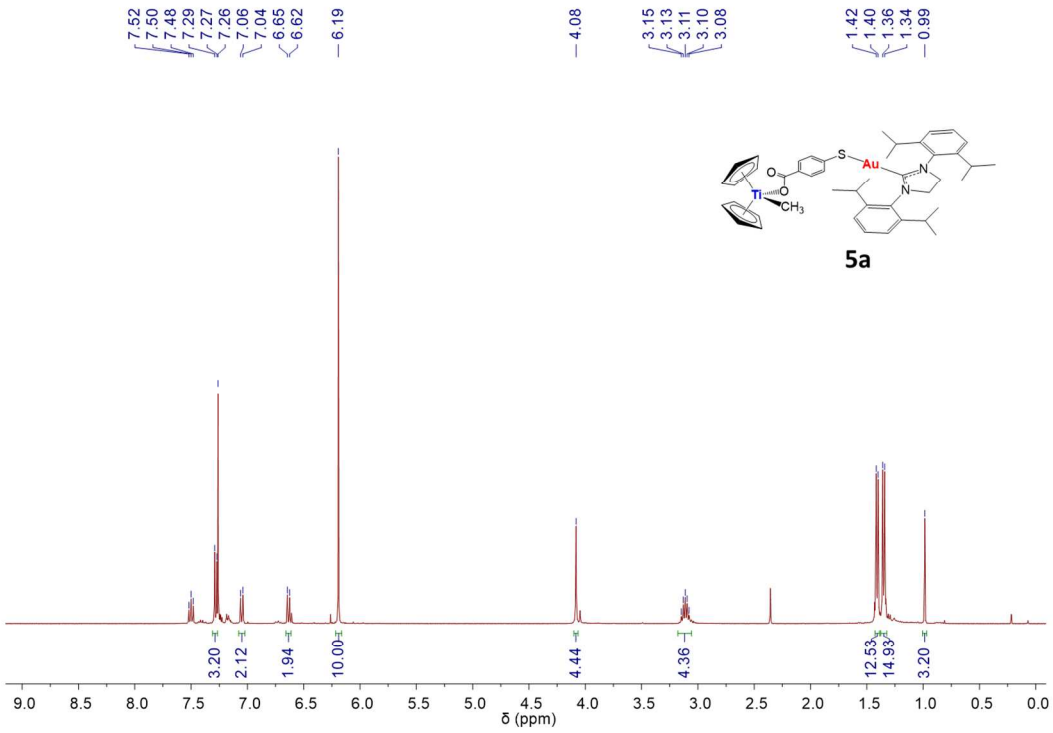


**Figure S9.** $^{1}H$ NMR spectrum of compound **5a** in $CDCl_3$.

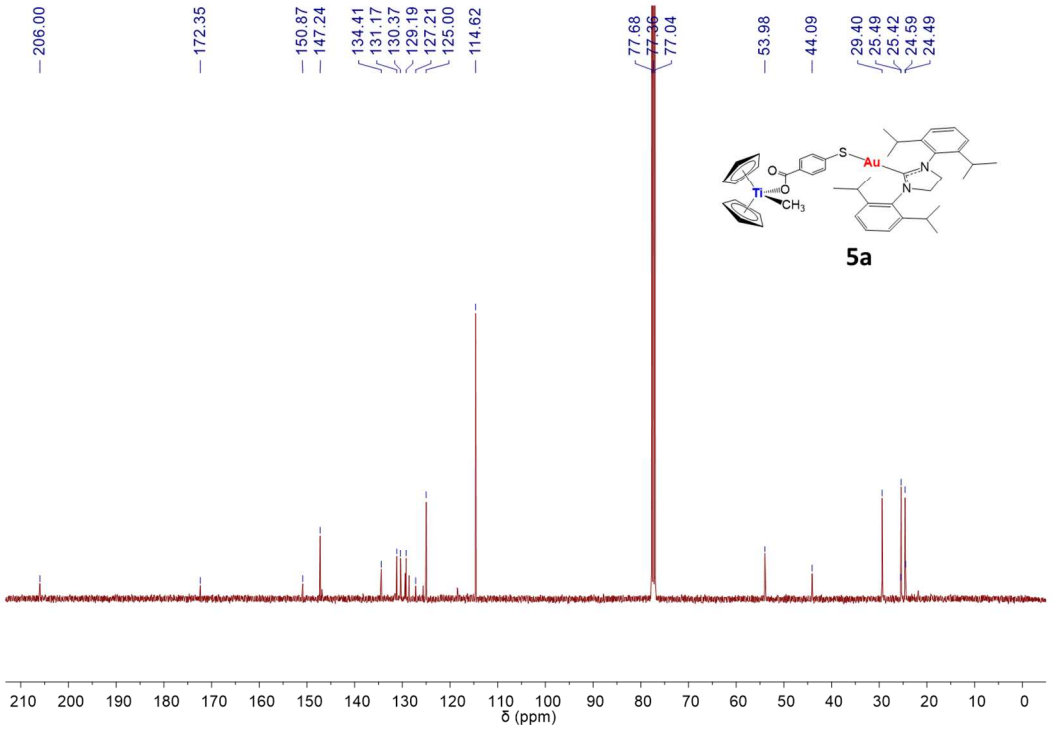


**Figure S10.** $^{13}C\{^{1}H\}$ NMR spectrum of compound **5a** in $CDCl_3$.

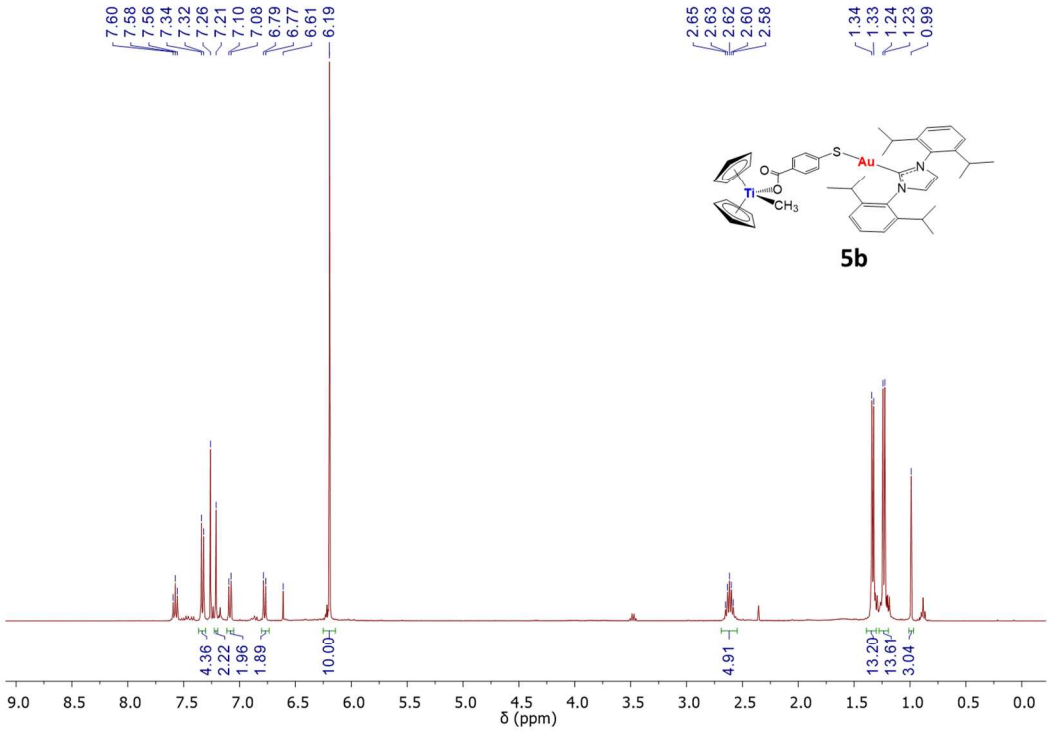


**Figure S11.** $^{1}H$ NMR spectrum of compound **5b** in $CDCl_3$.

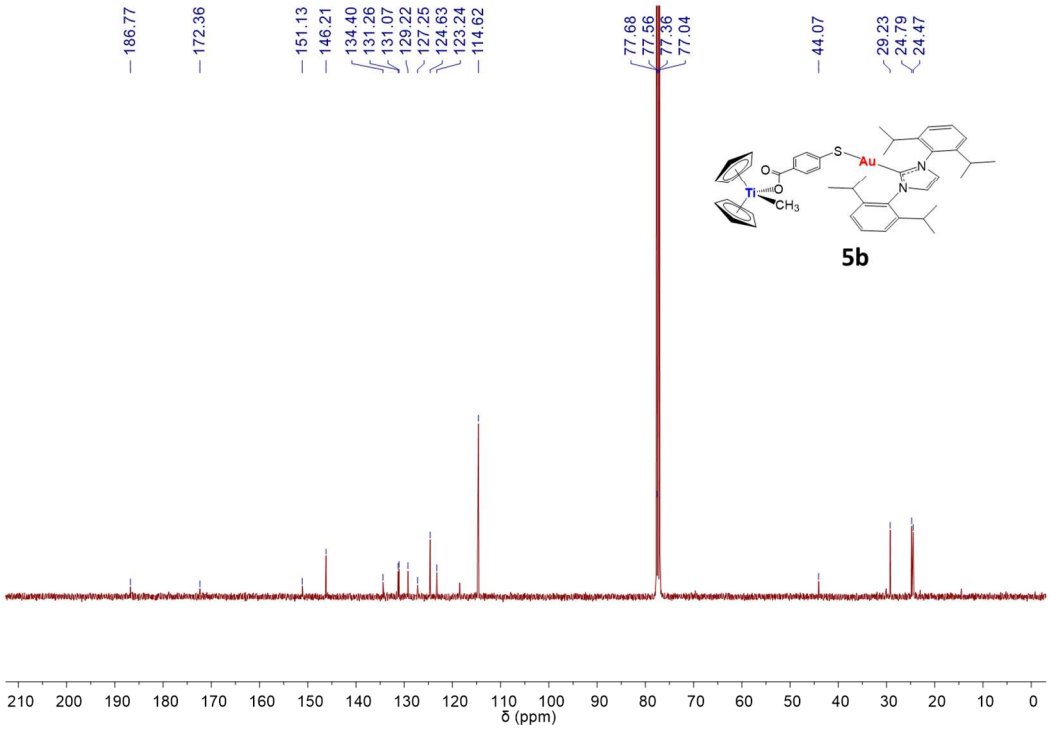


**Figure S12.** $^{13}C\{^{1}H\}$ NMR spectrum of compound **5b** in $CDCl_3$.

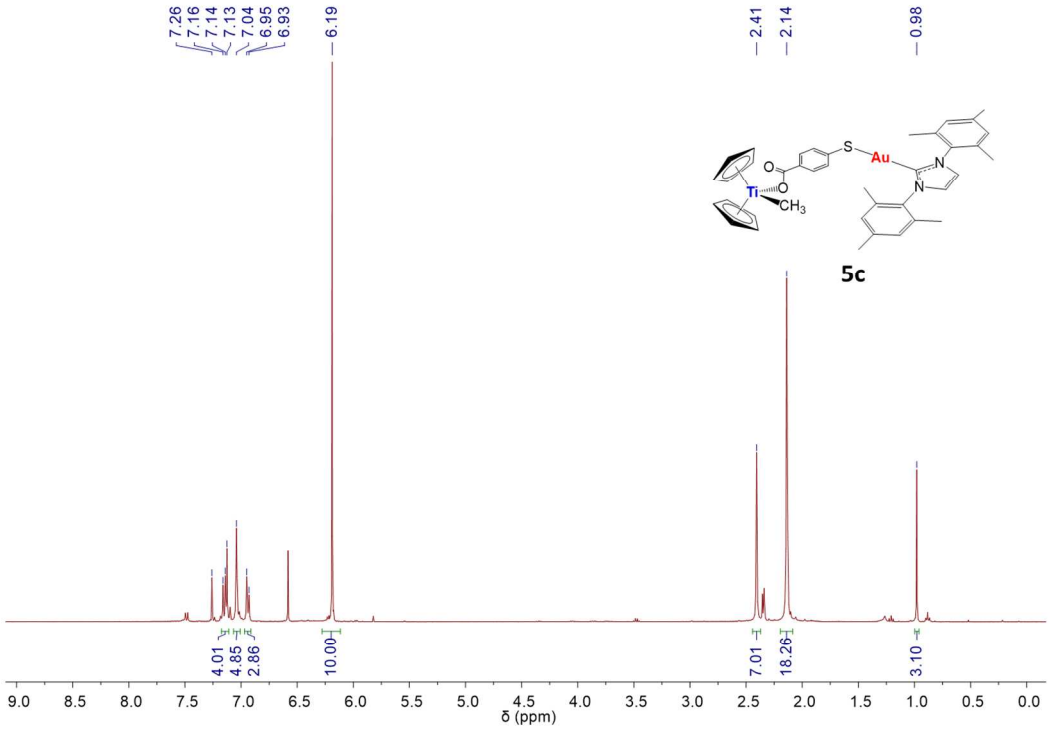


**Figure S13.** $^{1}H$ NMR spectrum of compound **5c** in $CDCl_3$.

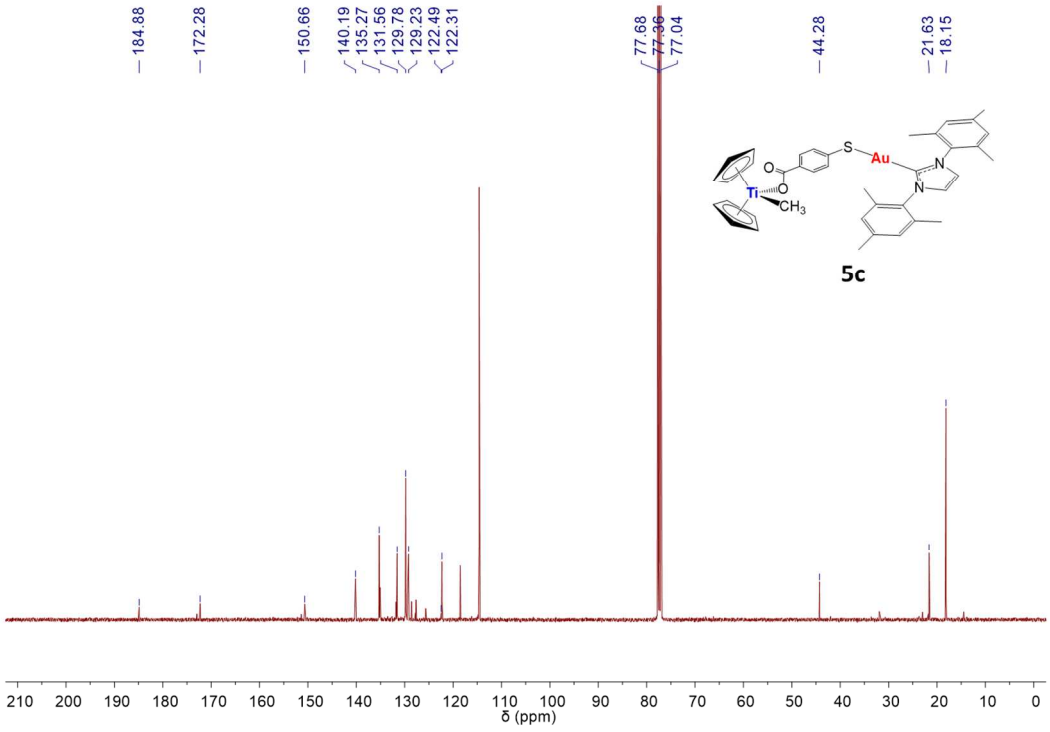


**Figure S14.** $^{13}C\{^{1}H\}$ NMR spectrum of compound **5c** in $CDCl_3$.

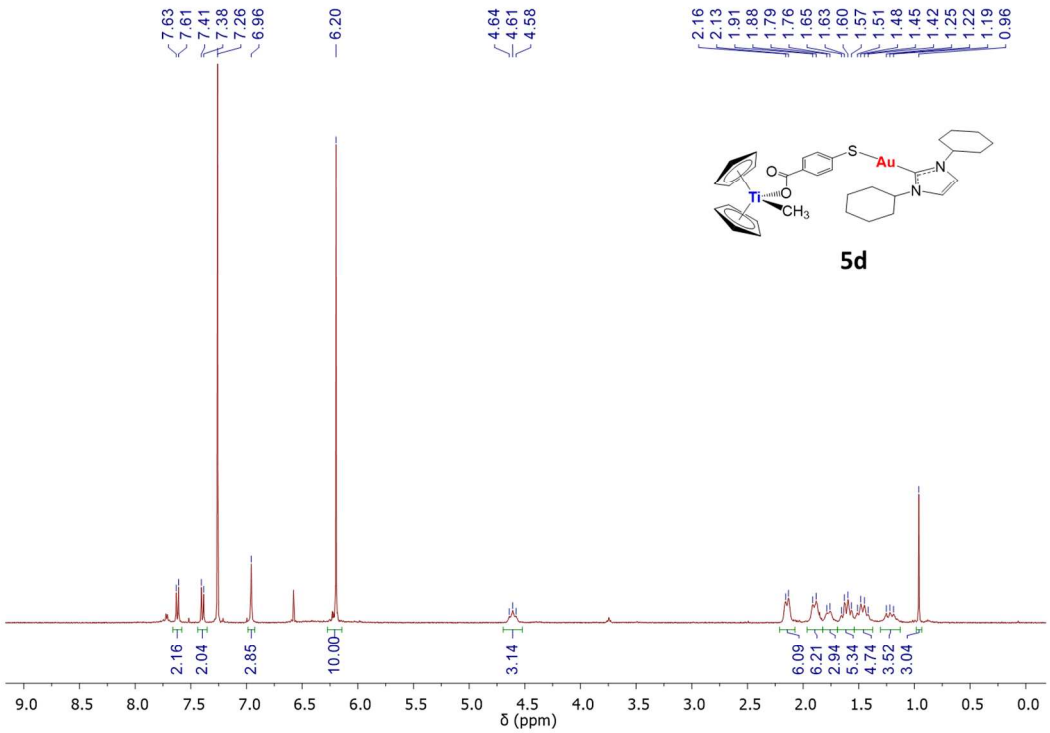


**Figure S15.** $^{1}H$ NMR spectrum of compound **5d** in $CDCl_3$.

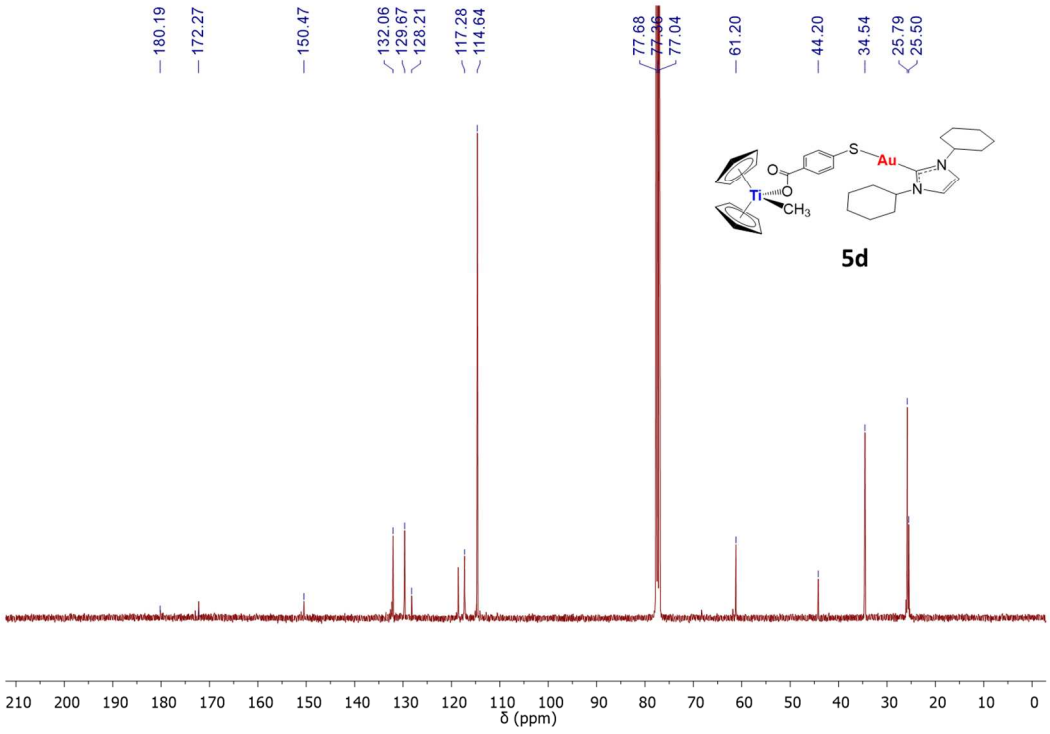


**Figure S16.** $^{13}C\{^{1}H\}$ NMR spectrum of compound **5d** in $CDCl_3$.

**2.** NMR spectra of decomposition of compounds **5a-d** in DMSO-$d_6$ and in DMSO-$d_6$/PBS-$D_2O$

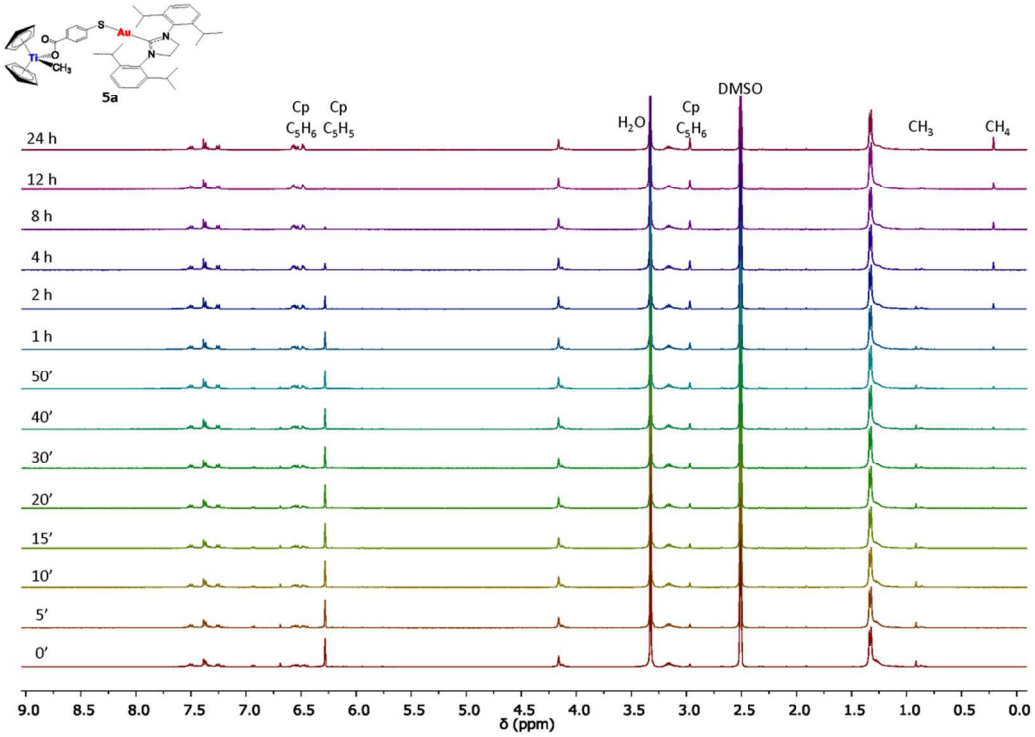


**Figure S17**. Time course $^1$H NMR spectrum in DMSO-$d_6$ of compound **5a**. $t_{½}$ = 1h.

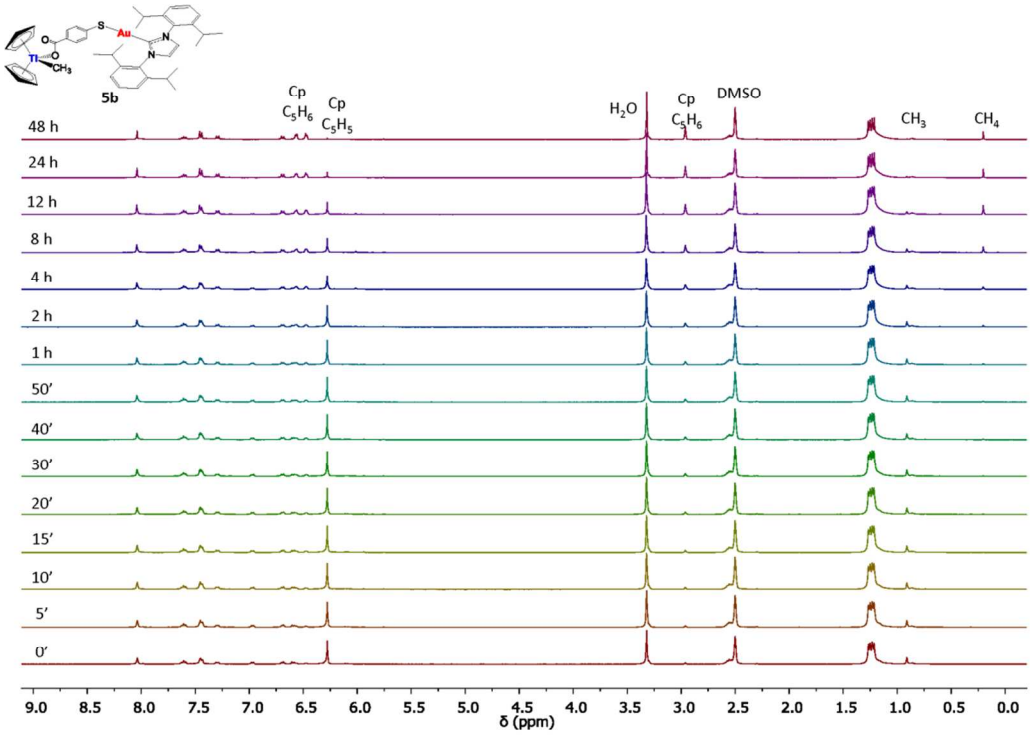


**Figure S18**. Time course $^1$H NMR spectrum in DMSO-$d_6$ of compound **5b**. $t_{½}$ = 3h.

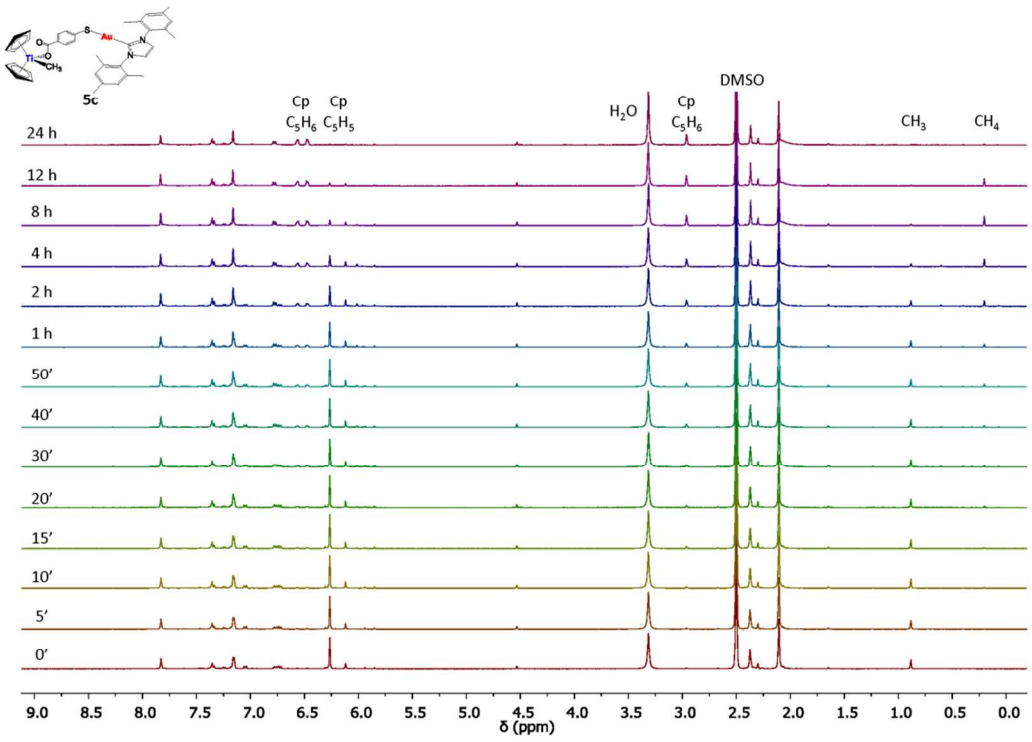


**Figure S19**. Time course $^{1}$H NMR spectrum in DMSO-$d_6$ of compound **5c**. $t_{½}$ = 2h.

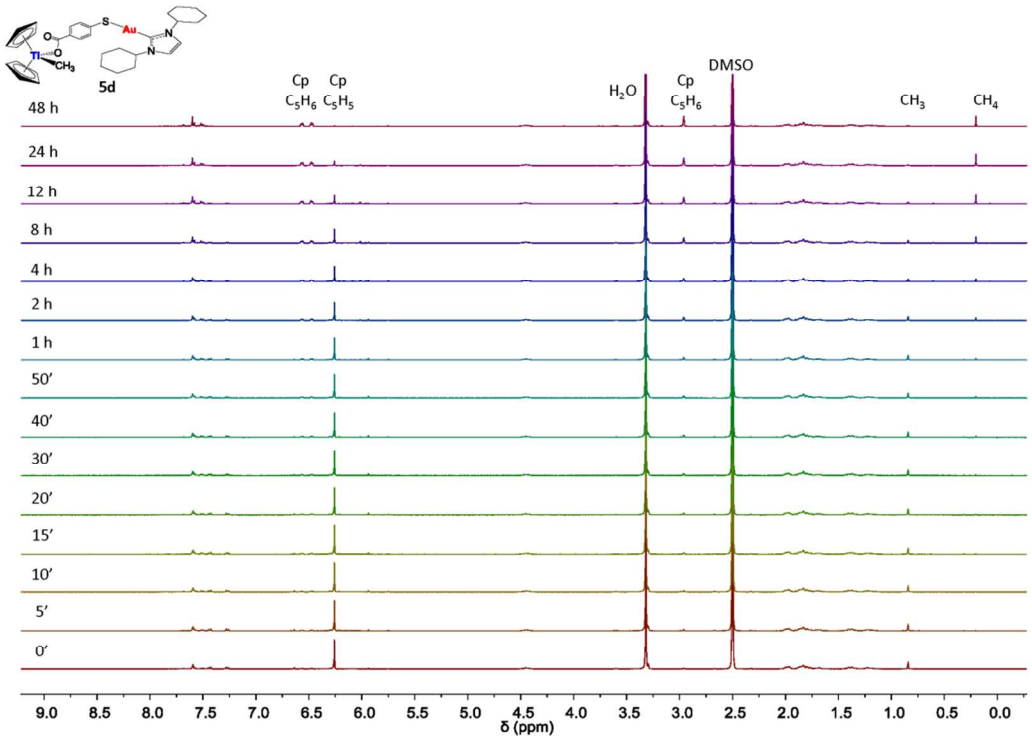


**Figure S20**. Time course $^{1}$H NMR spectrum in DMSO-$d_6$ of compound **5d**. $t_{½}$ = 2h.

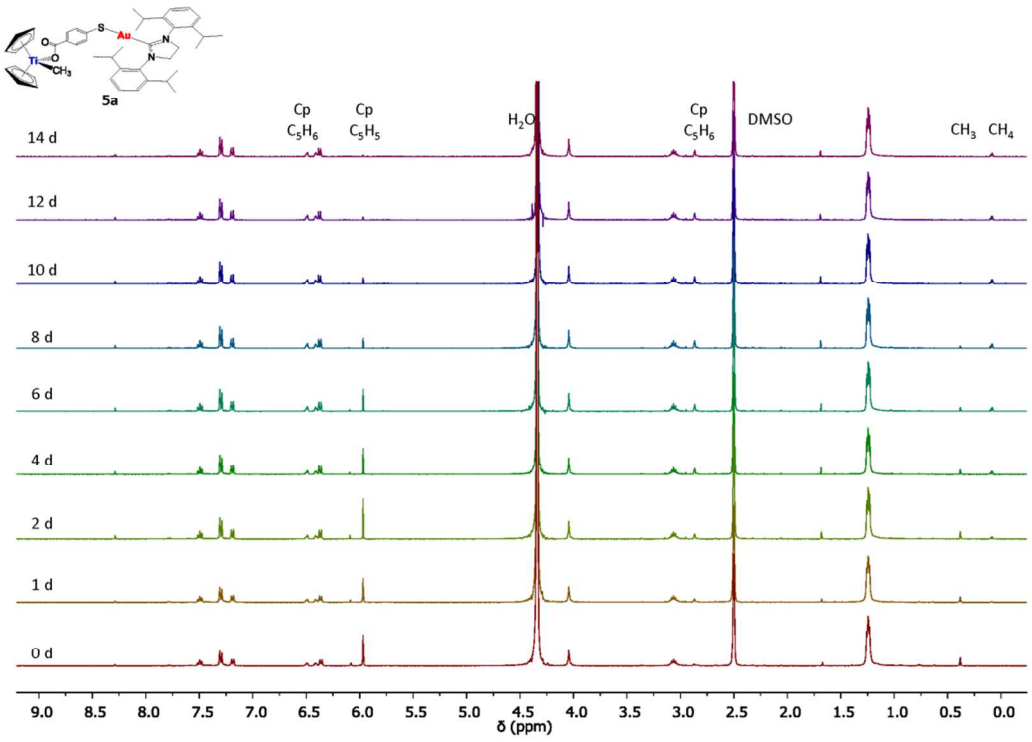


**Figure S21**. Time course $^{1}$H NMR spectrum in 3:2 DMSO-$d_6$/PBS-$D_2O$ of compound **5a**. $t_{½}$ = 24h.

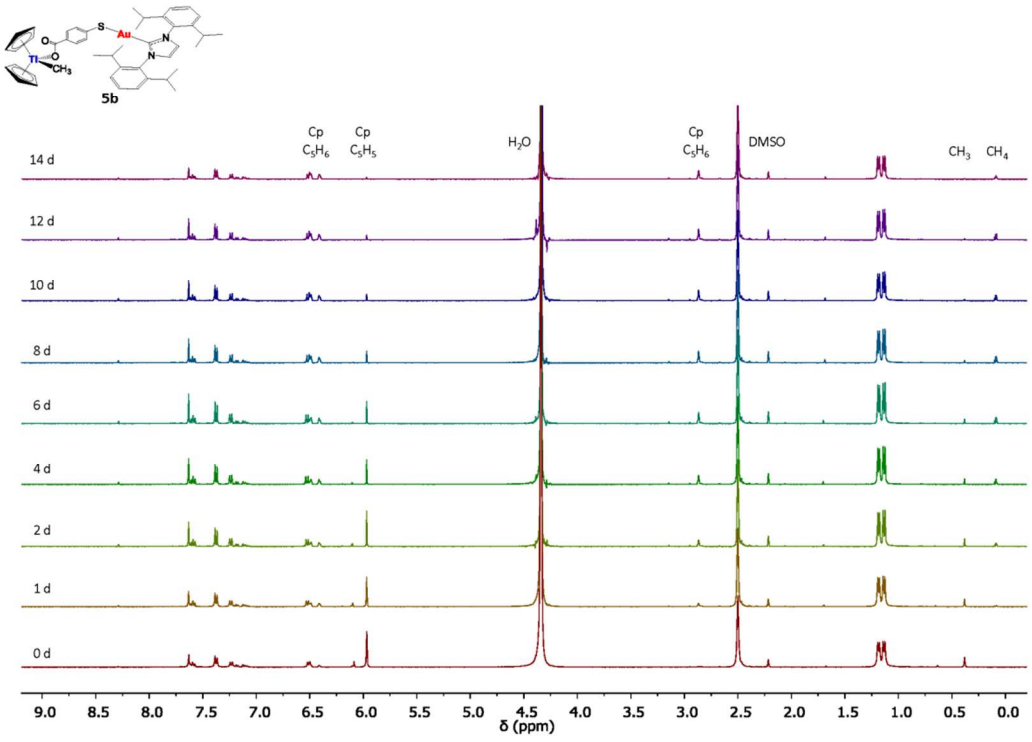


**Figure S22**. Time course $^{1}$H NMR spectrum in 3:2 DMSO-$d_6$/PBS-$D_2O$ of compound **5b**. $t_{½}$ = 24h.

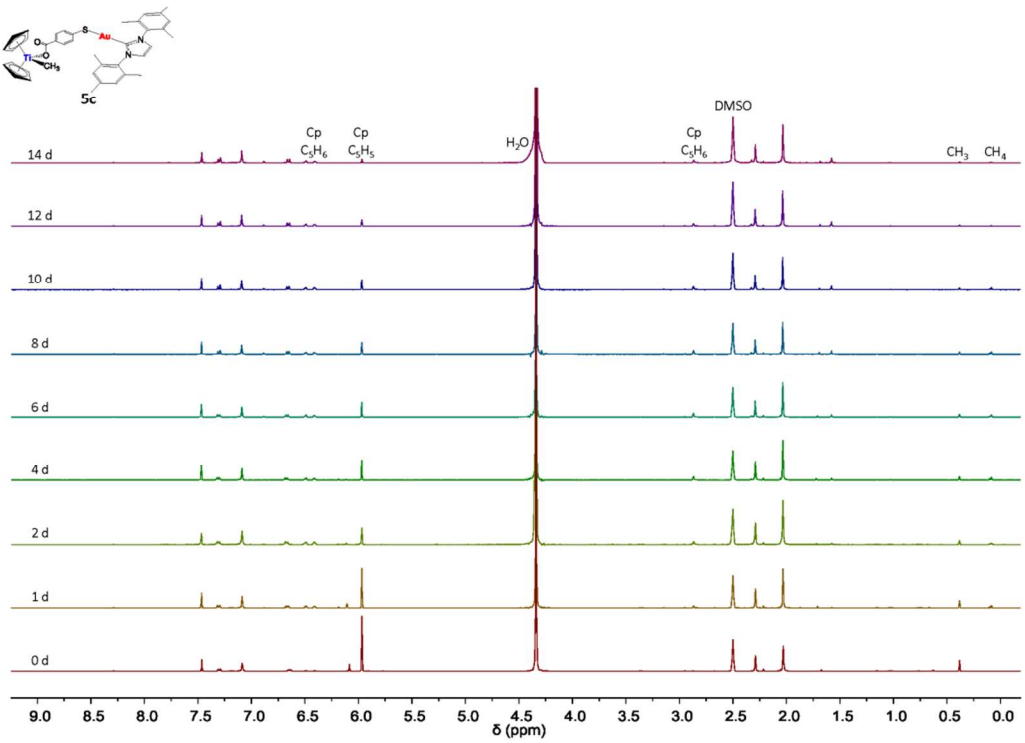


**Figure S23**. Time course $^1$H NMR spectrum in 3:2 DMSO-$d_6$/PBS-$D_2O$ of compound **5c**. $t_{½}$ = 24h.

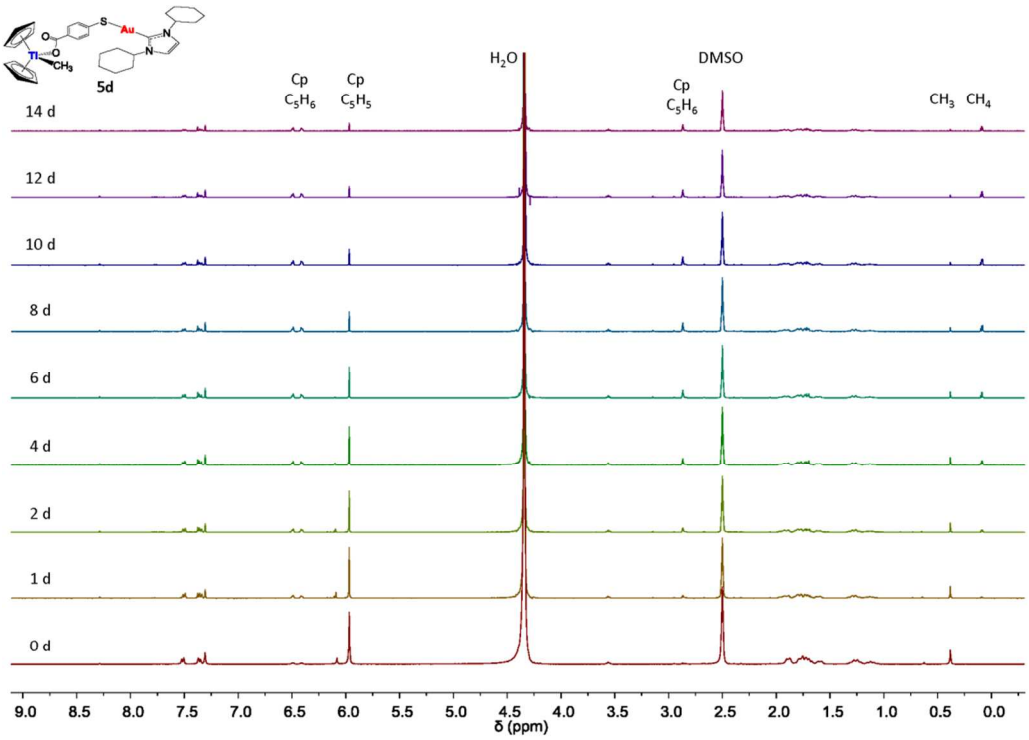


**Figure S24**. Time course $^1$H NMR spectrum in 3:2 DMSO-$d_6$/PBS-$D_2O$ of compound **5d**. $t_{½}$ = 48h.

**3.** MS ESI+ spectra of all compounds and theoretical isotopic distributions of relevant peaks

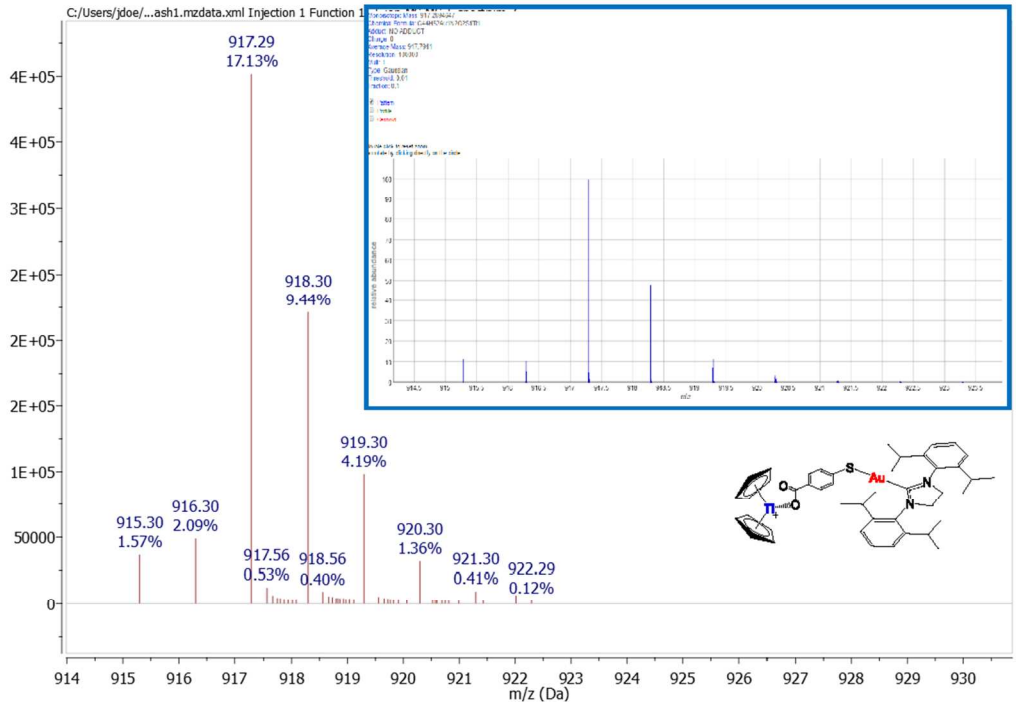


**Figure S25**. Magnification of peak at [m/z]: 917.29 in MS ESI+ of compound **5a** in 1% DMSO/$H_2O$ solution at t=0. Insert: theoretical isotopic distribution.

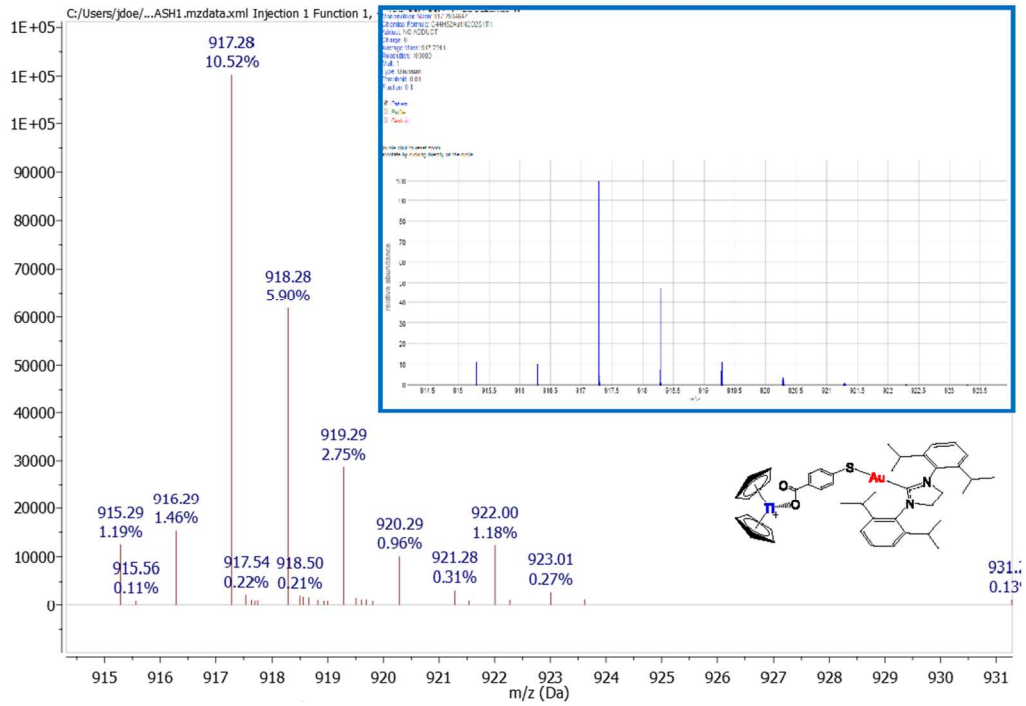


**Figure S26**. Magnification of peak at [m/z]: 917.29 in MS ESI+ of compound **5a** in 1% DMSO/$H_2O$ solution at t=24h. Insert: theoretical isotopic distribution.

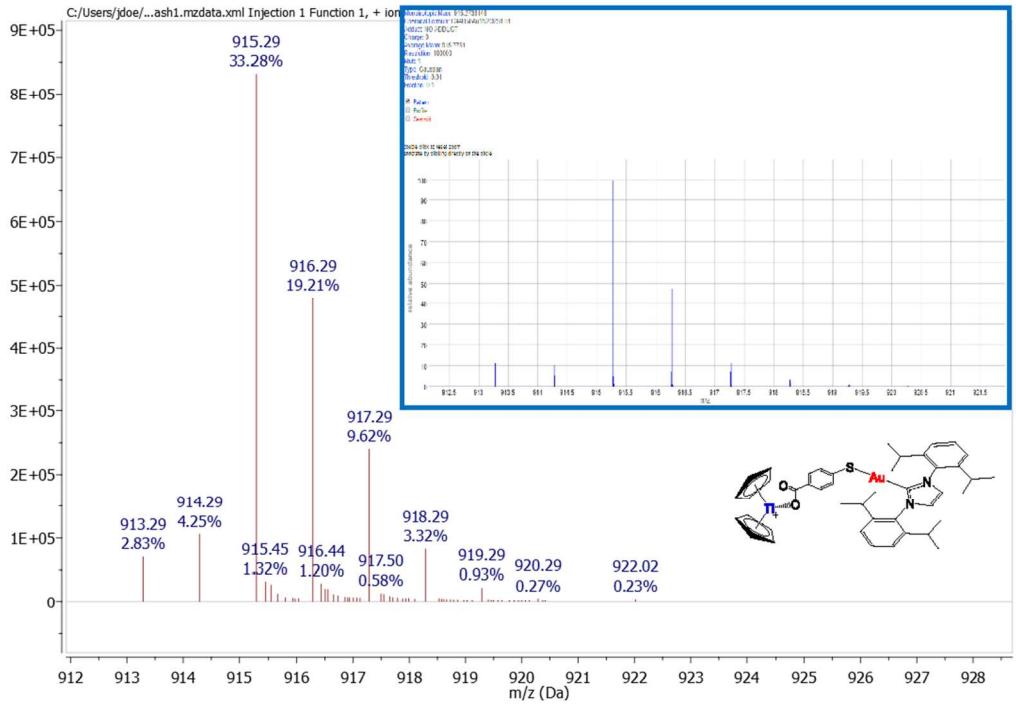


**Figure S27**. Magnification of peak at [m/z]: 915.21 in MS ESI+ of compound **5b** in 1% DMSO/$H_2O$ solution at t=0. Insert: theoretical isotopic distribution.

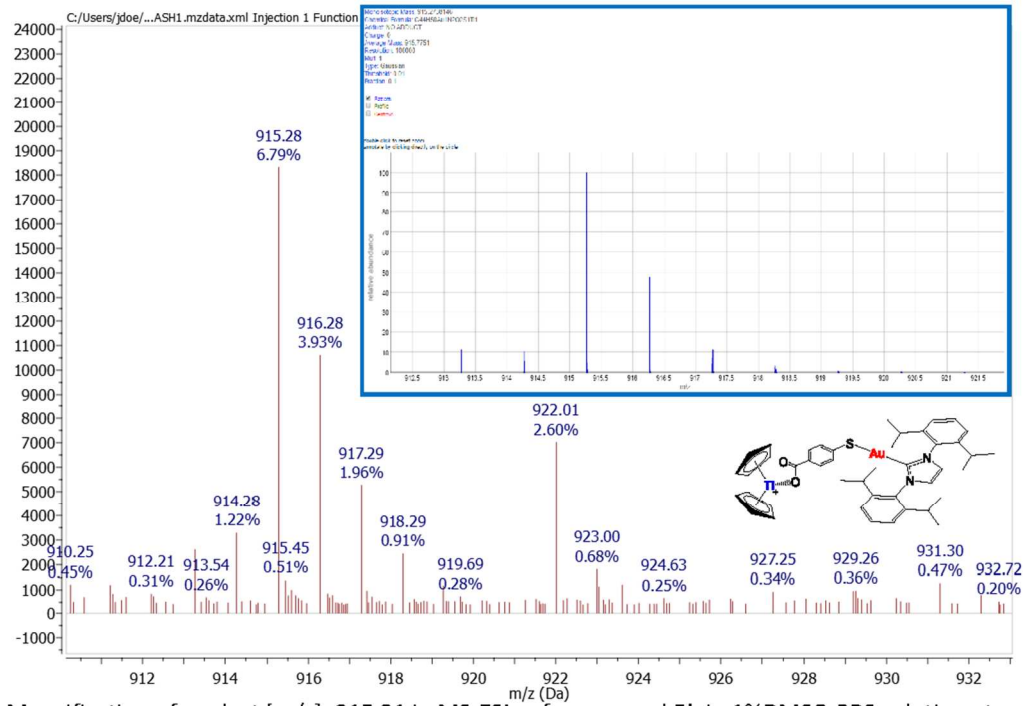


**Figure S28**. Magnification of peak at [m/z]: 915.21 in MS ESI+ of compound **5b** in 1% DMSO/$H_2O$ solution at t=24h. Insert: theoretical isotopic distribution.

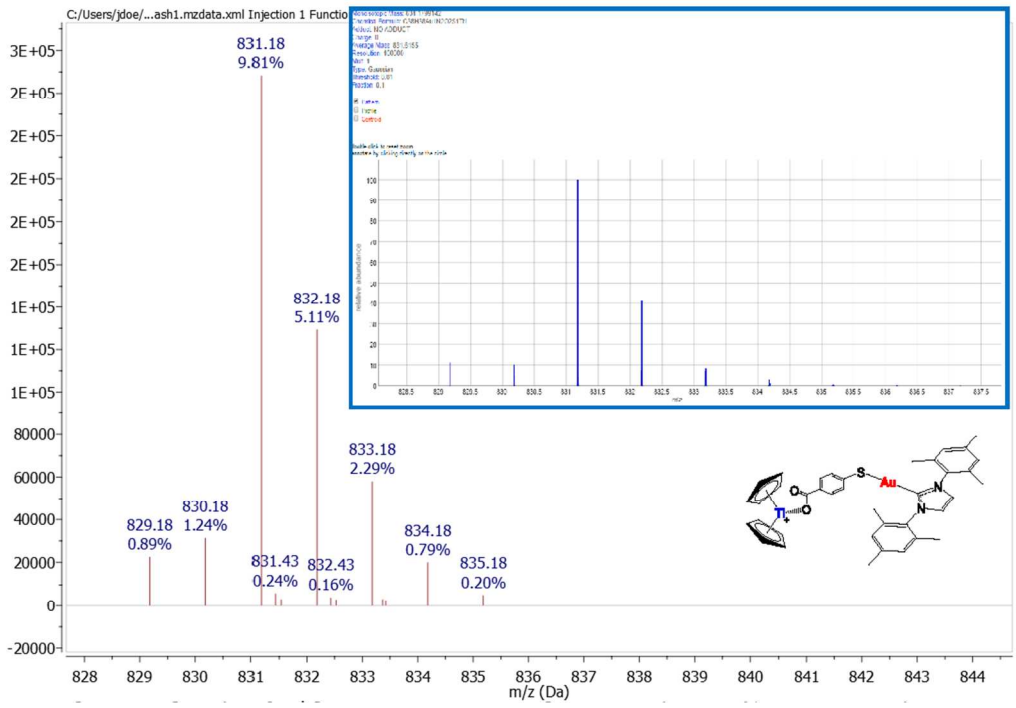


**Figure S29**. Magnification of peak at [m/z]: 831.16 in MS ESI+ of compound **5c** in 1% DMSO/$H_2O$ solution at t=0. Insert: theoretical isotopic distribution.

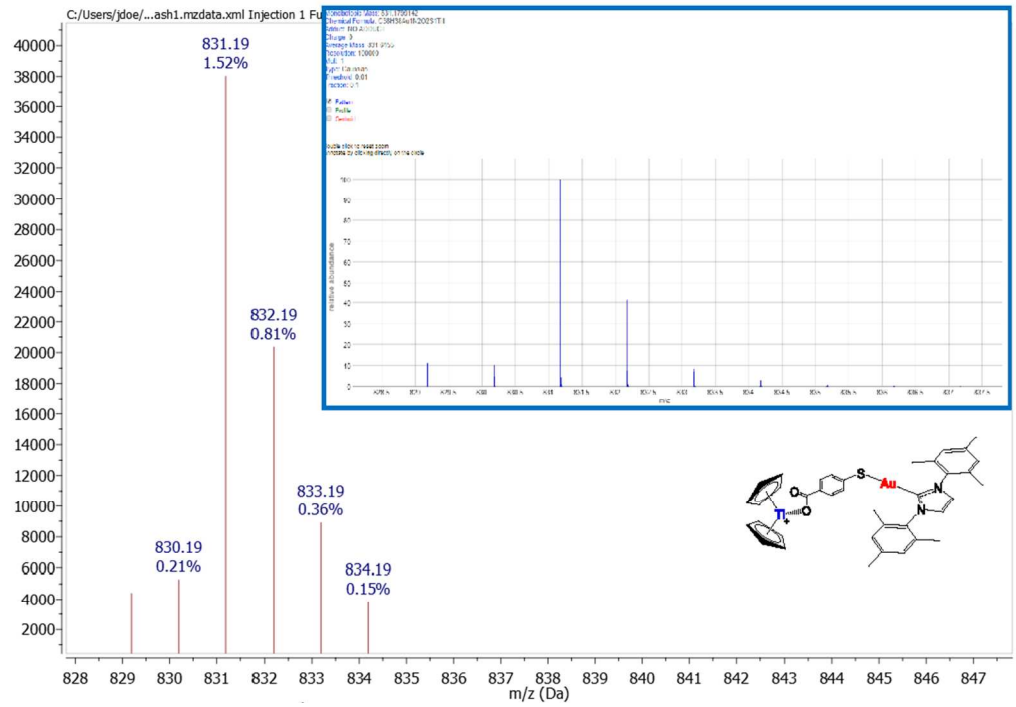


**Figure S30**. Magnification of peak at [m/z]: 831.16 in MS ESI+ of compound **5c** in 1% DMSO/$H_2O$ solution at t=24h. Insert: theoretical isotopic distribution.

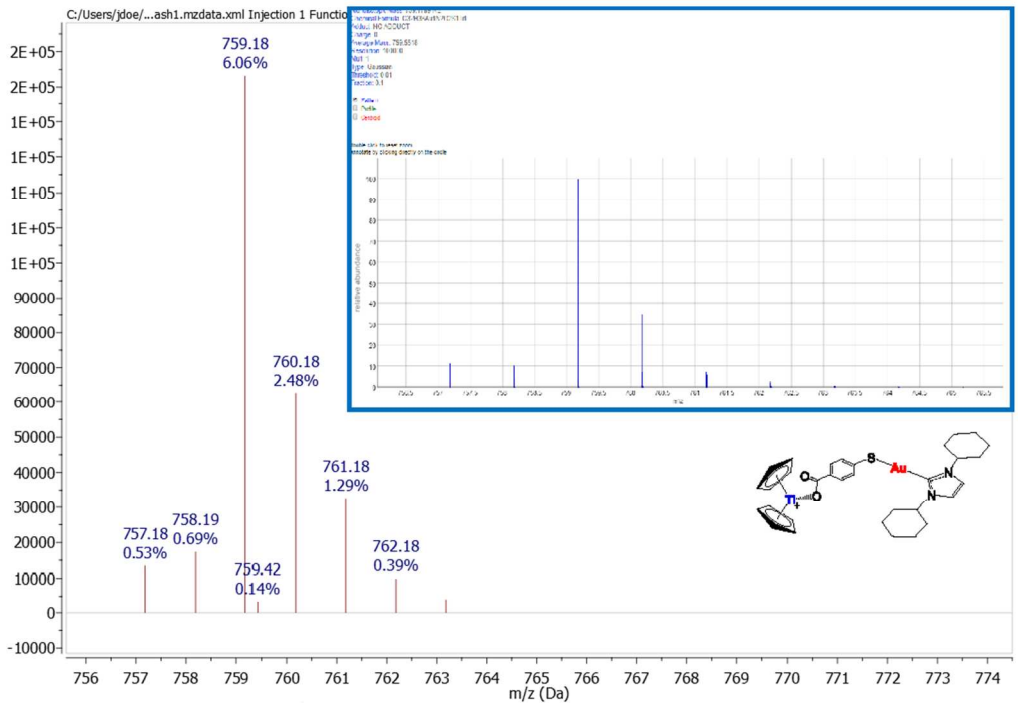


**Figure S31**. Magnification of peak at [m/z]: 759.16 in MS ESI+ of compound **5d** in 1% DMSO/$H_2O$ solution at t=0. Insert: theoretical isotopic distribution.

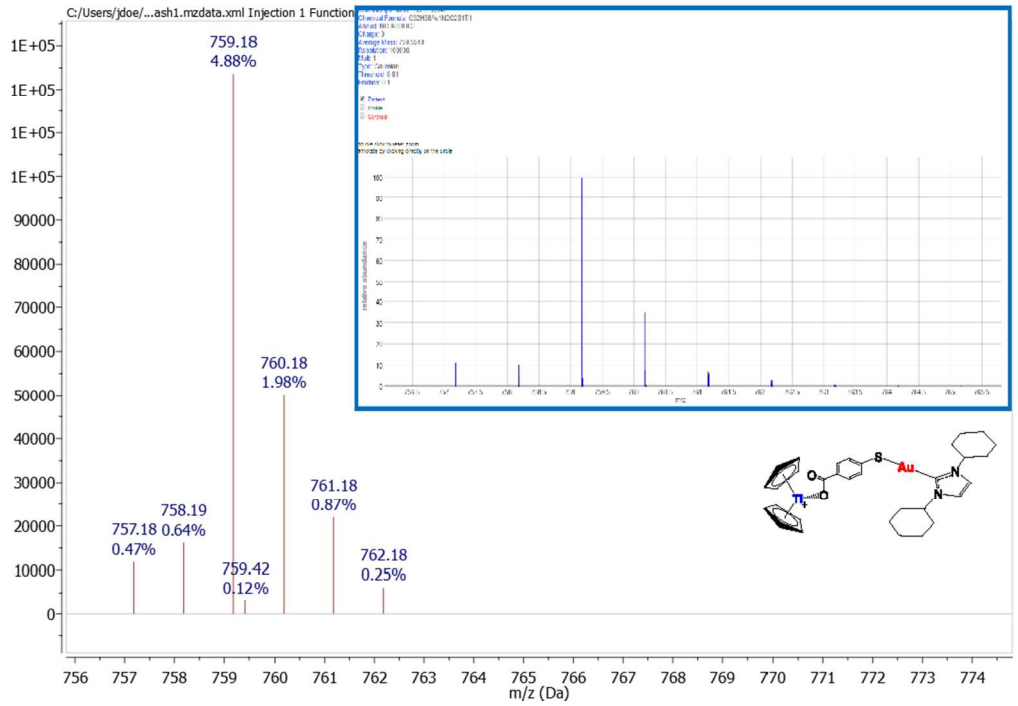


**Figure S32**. Magnification of peak at [m/z]: 759.16 in MS ESI+ of compound **5d** in 1% DMSO/$H_2O$ solution at t=24h. Insert: theoretical isotopic distribution.

**4.** Solid state IR spectra of all compounds

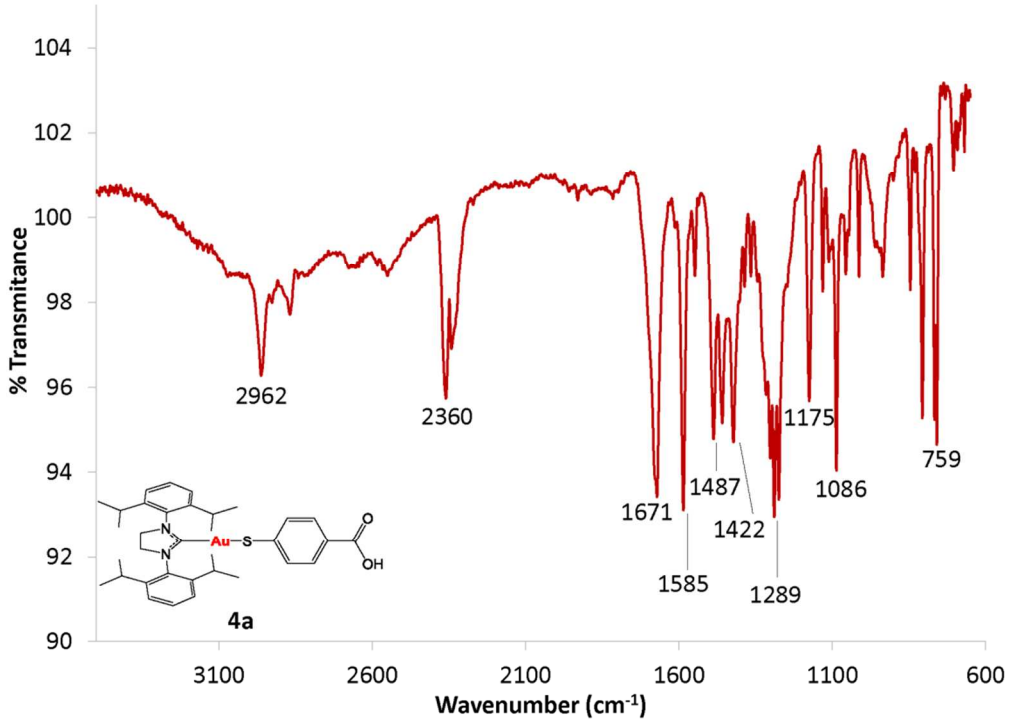


**Figure S33.** IR spectrum of compound **4a** in solid state at RT.

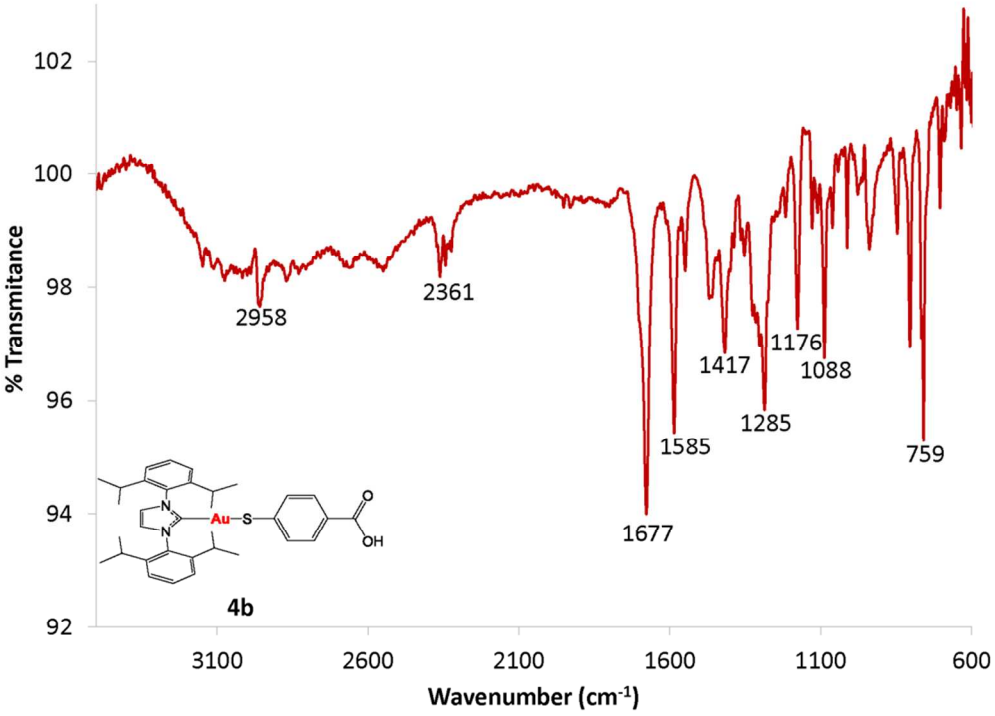


**Figure S34.** IR spectrum of compound **4b** in solid state at RT.

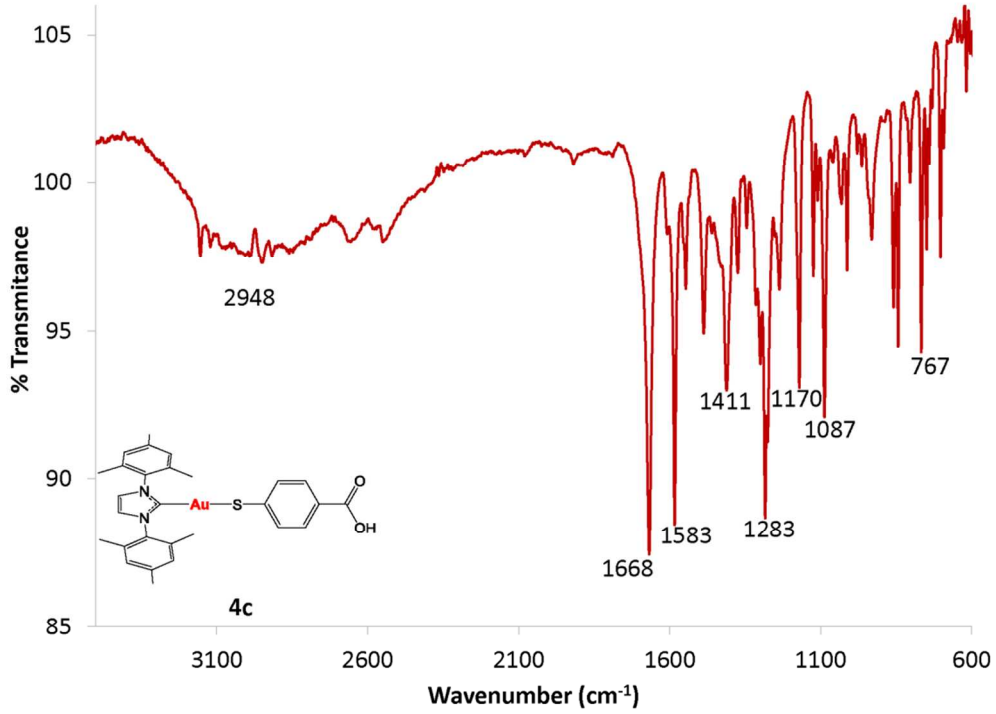


**Figure S35.** IR spectrum of compound **4c** in solid state at RT.

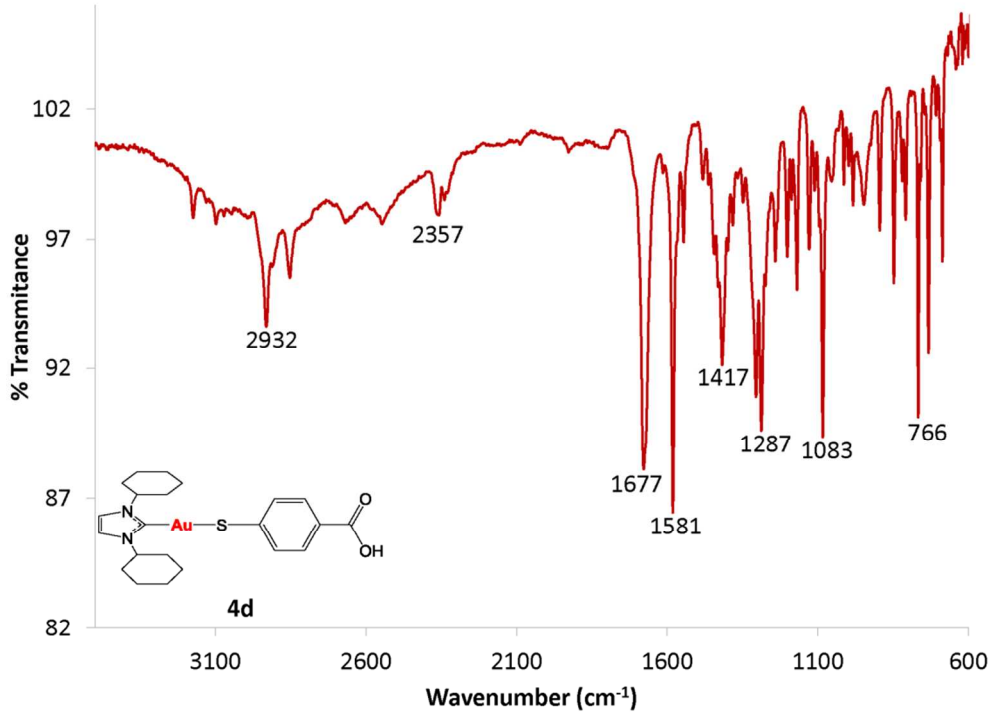


**Figure S36.** IR spectrum of compound **4d** in solid state at RT.

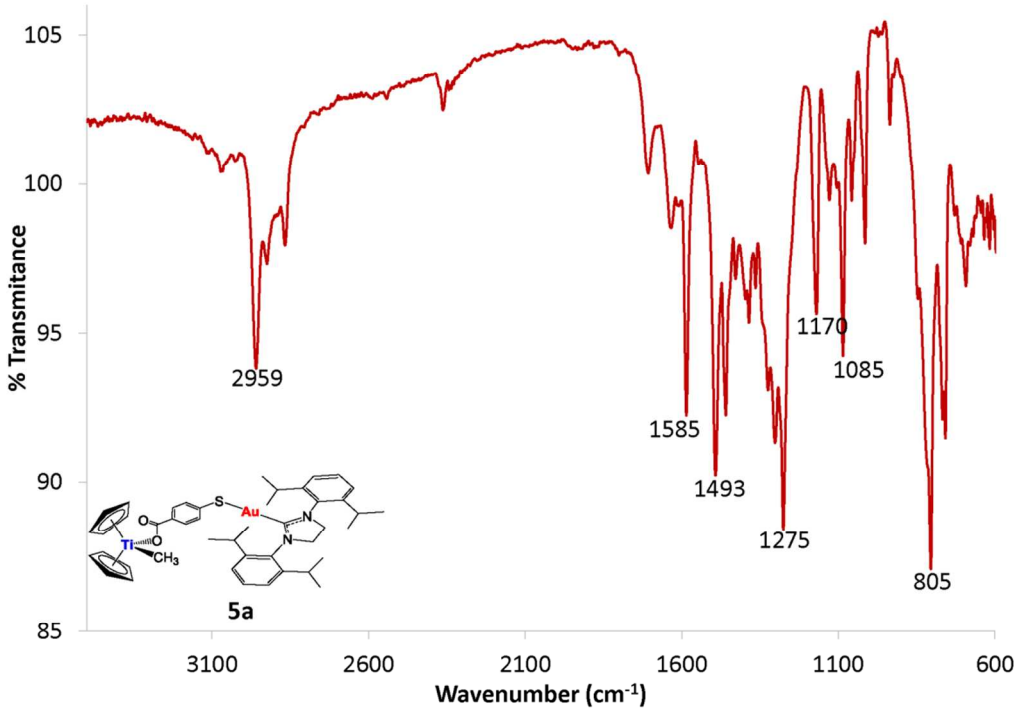


**Figure S37.** IR spectrum of compound **5a** in solid state at RT.

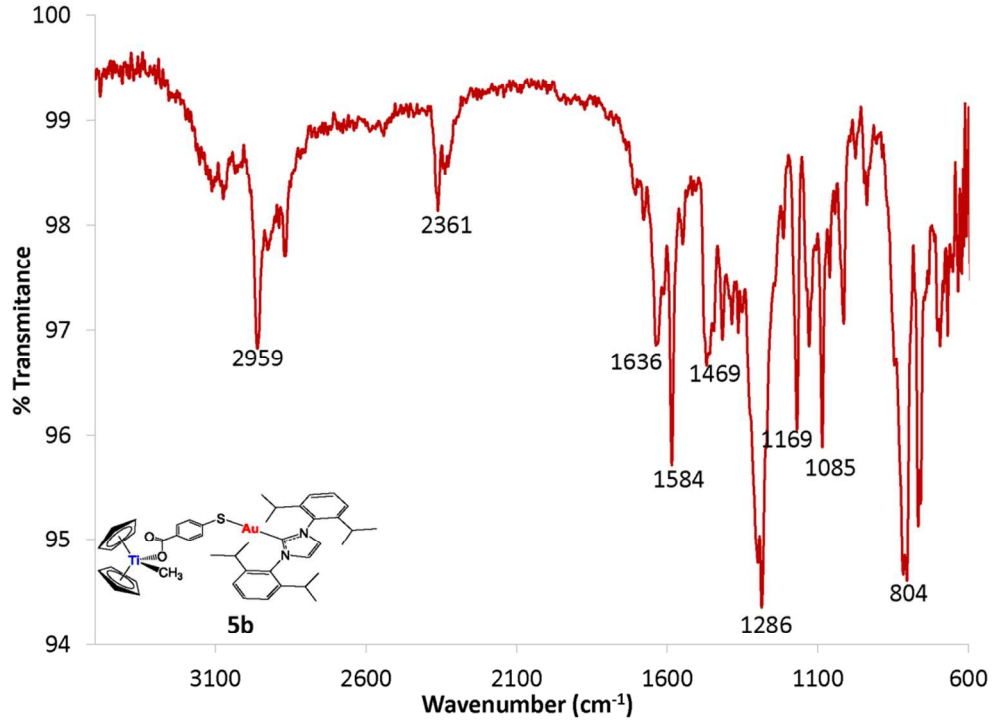


**Figure S38.** IR spectrum of compound **5b** in solid state at RT.

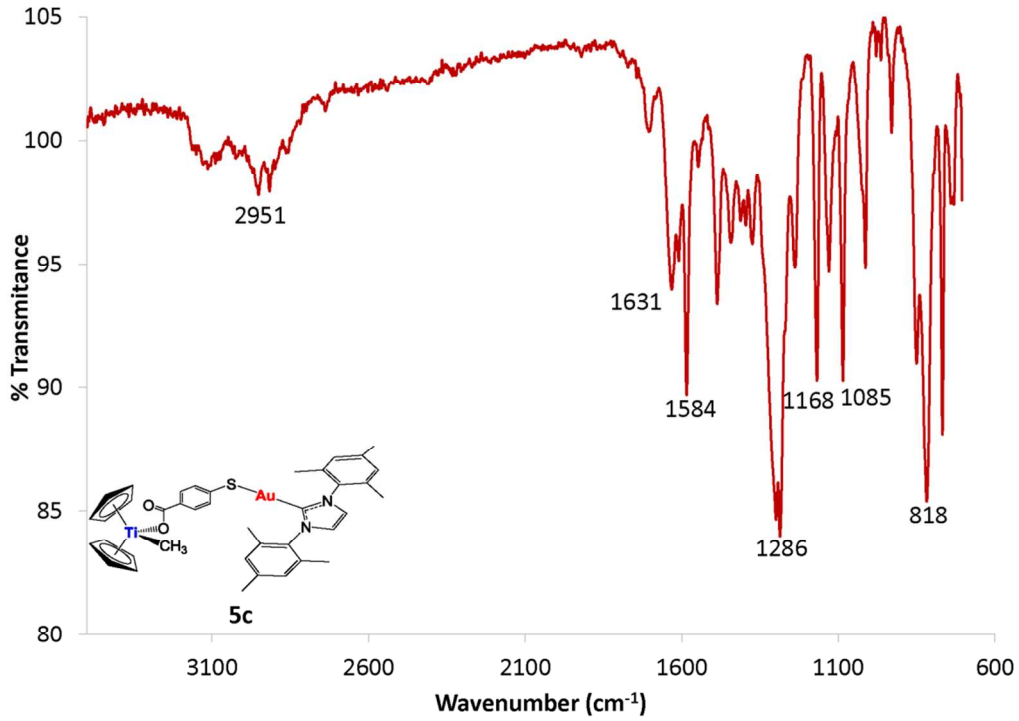


**Figure S39.** IR spectrum of compound **5c** in solid state at RT.

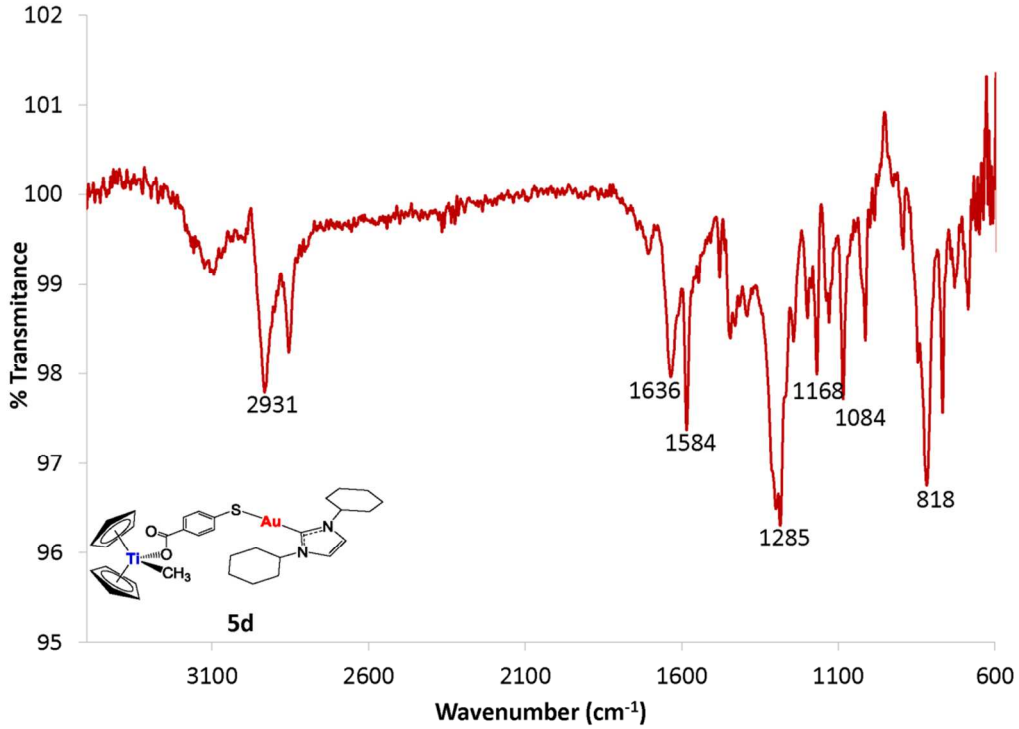


**Figure S40.** IR spectrum of compound **5d** in solid state at RT.

**5.** UV-visible spectra of compounds **4a-d** and **5a-d** in dichloromethane

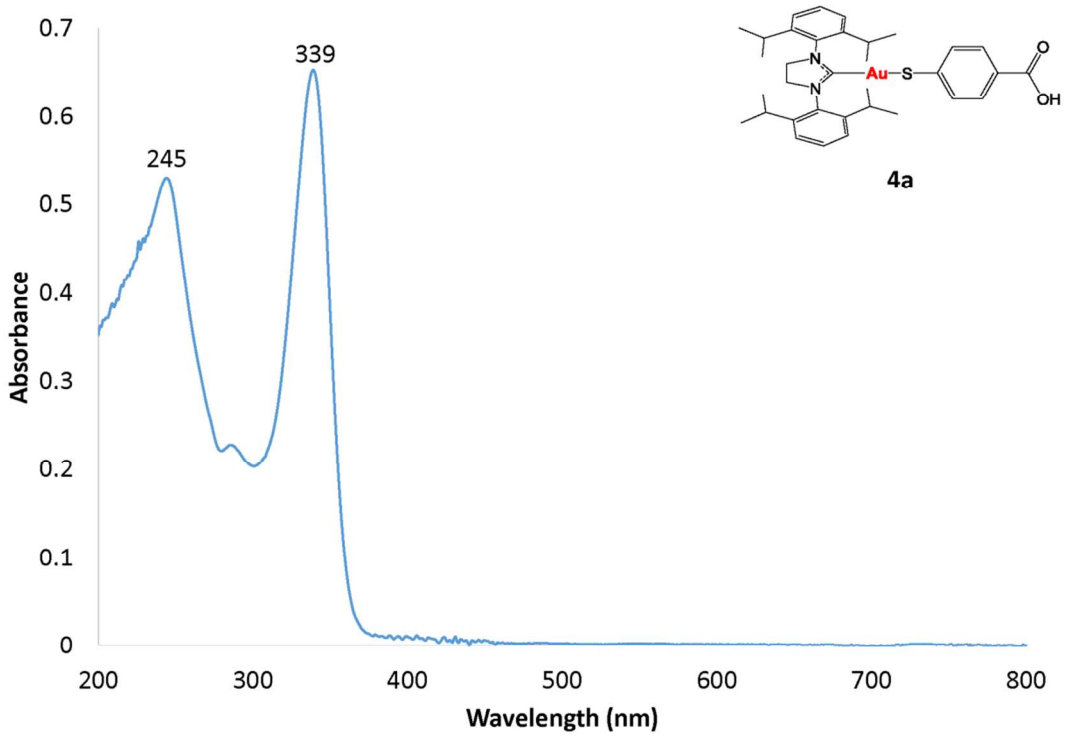


**Figure S41.** UV-visible spectrum of compound **4a** (2.00 $10^{-5}$ M) in dichloromethane.

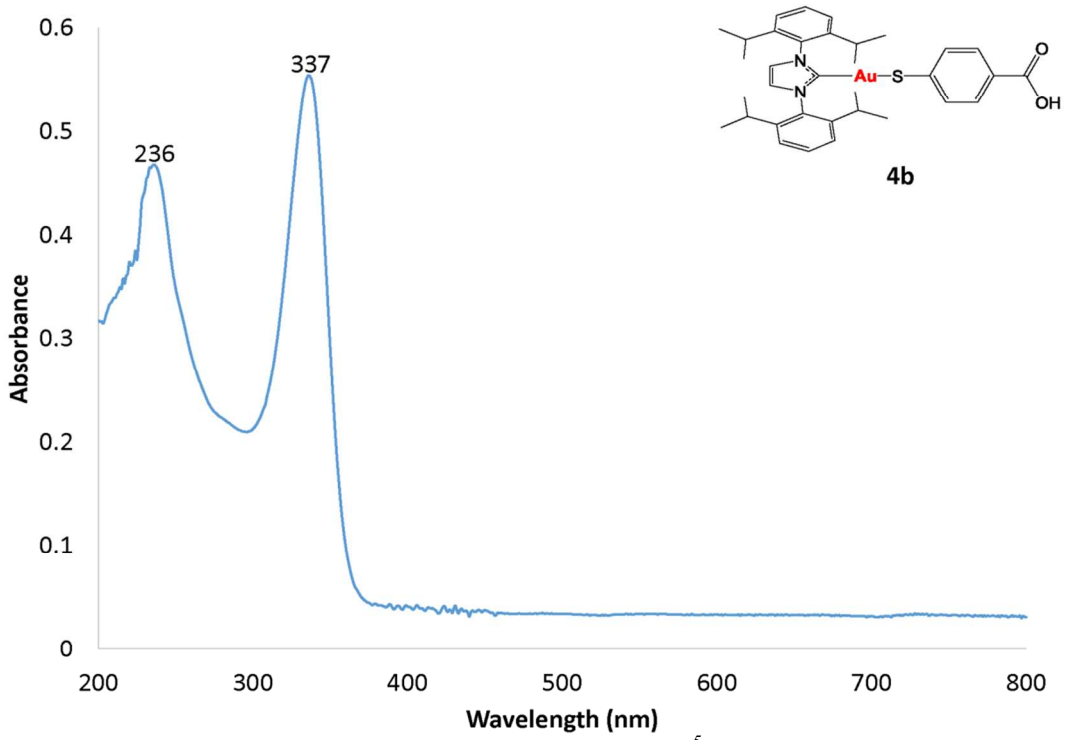


**Figure S42.** UV-visible spectrum of compound **4b** (2.00 $10^{-5}$ M) in dichloromethane.

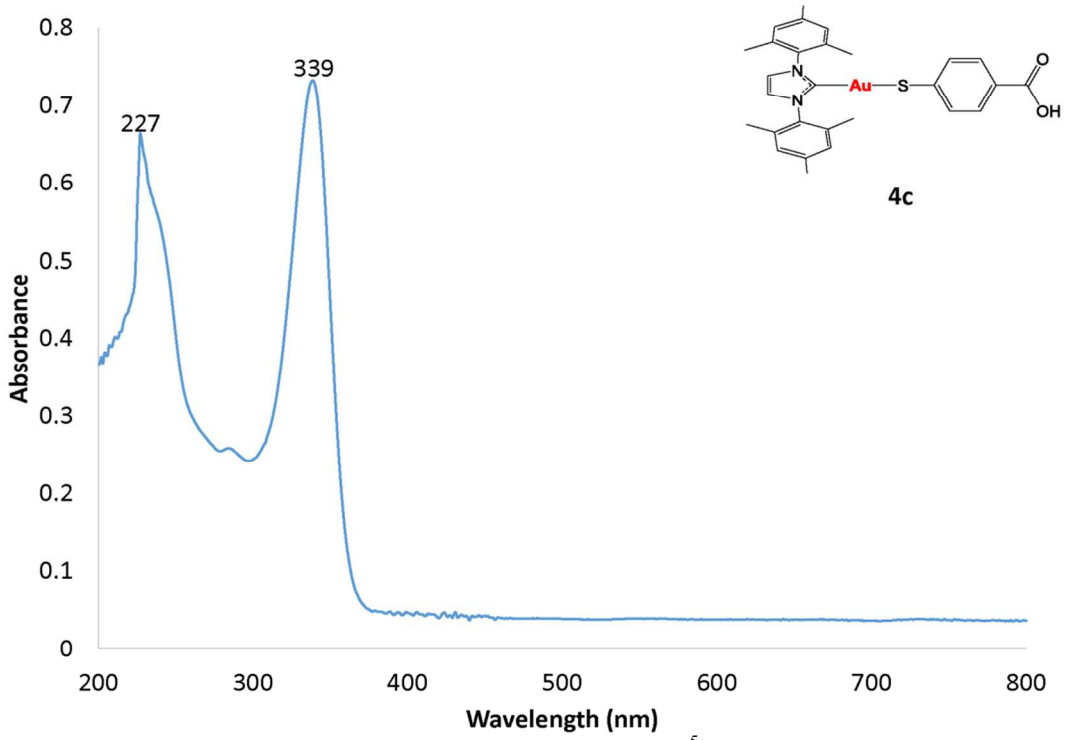


**Figure S43.** UV-visible spectrum of compound **4c** (2.18 $10^{-5}$ M) in dichloromethane.

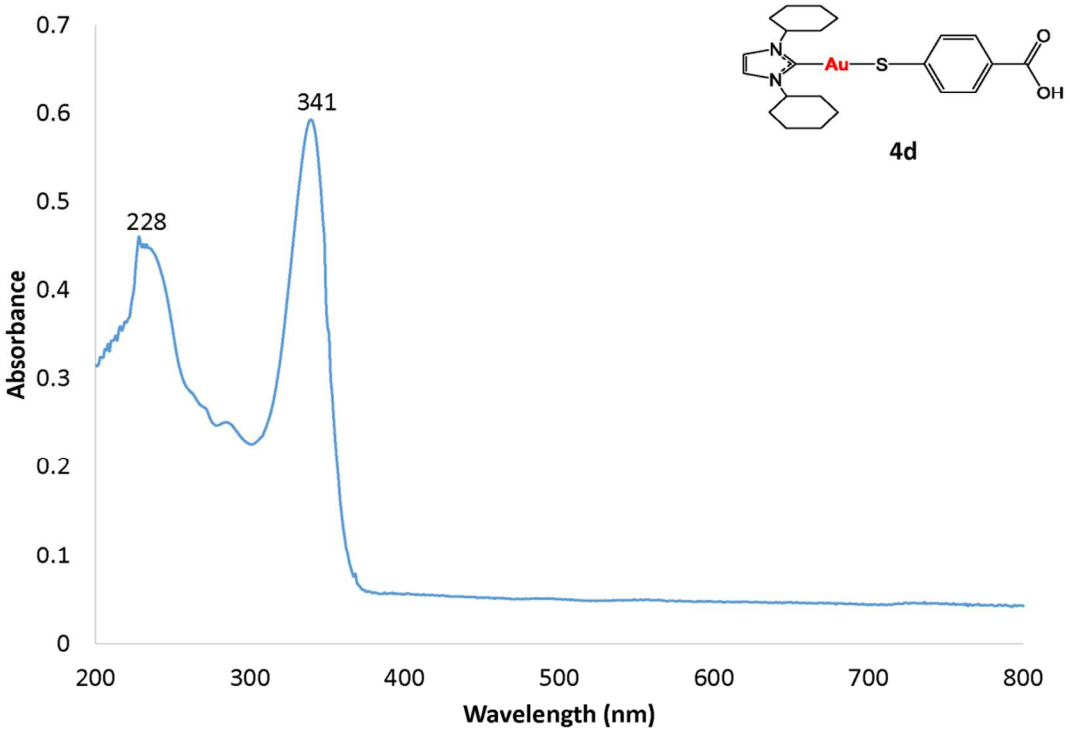


**Figure S44.** UV-visible spectrum of compound **4d** (2.35 $10^{-5}$ M) in dichloromethane.

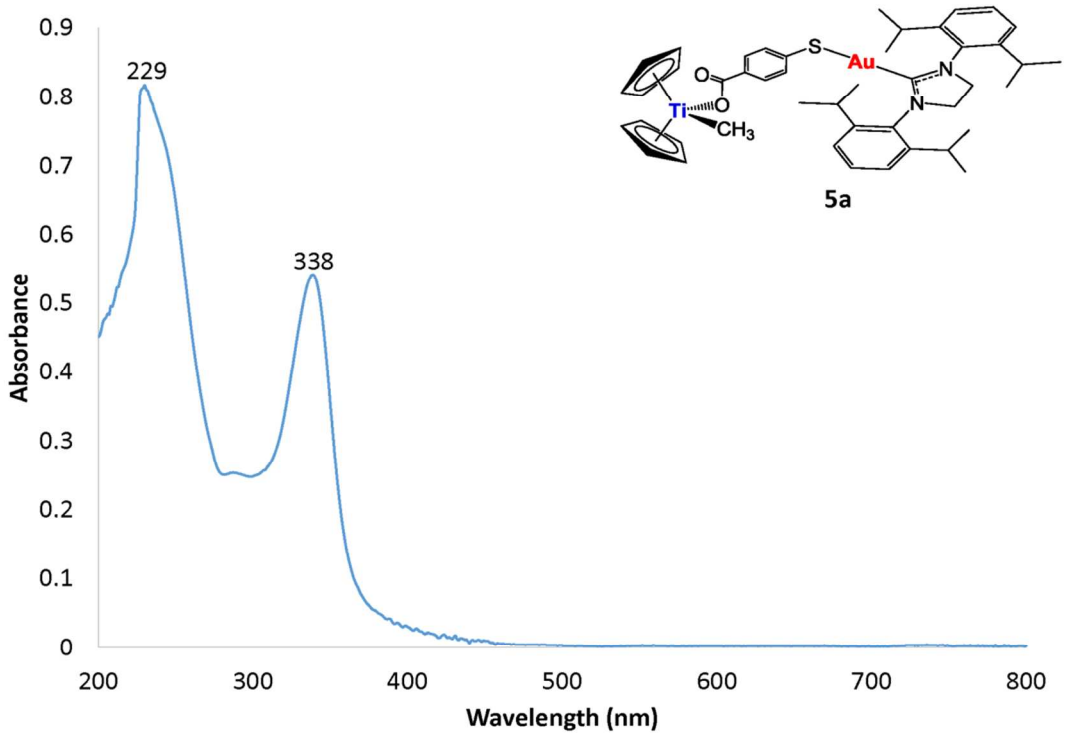


**Figure S45.** UV-visible spectrum of compound **5a** (3.22 $10^{-5}$ M) in dichloromethane.

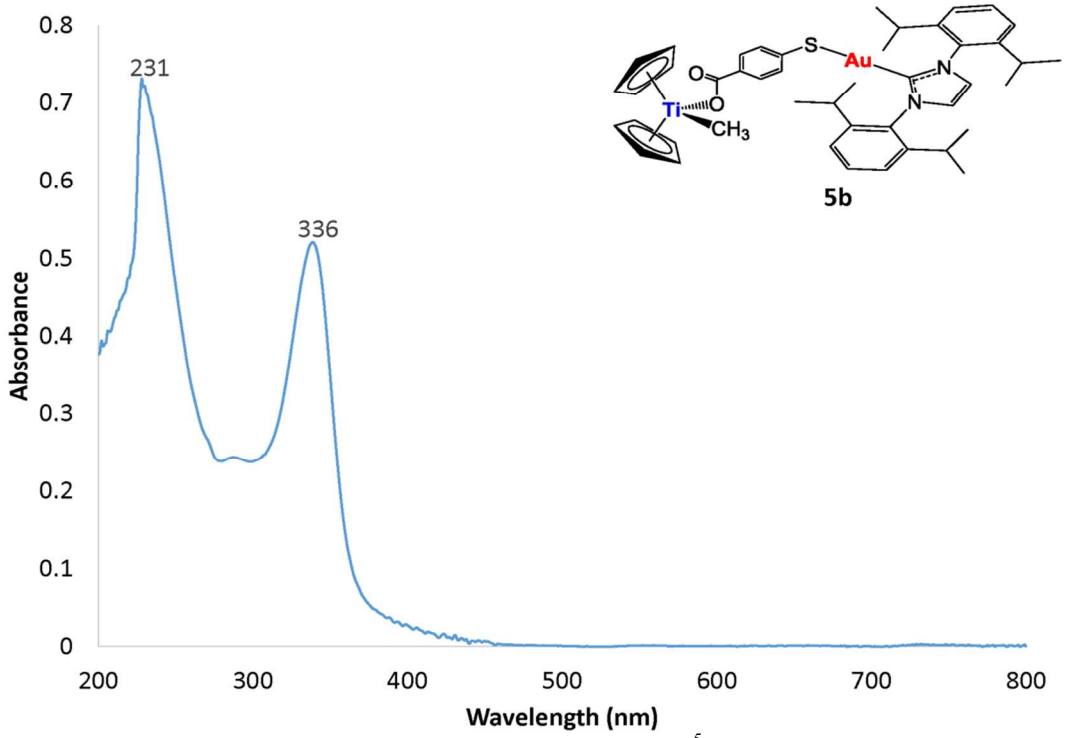


**Figure S46.** UV-visible spectrum of compound **5b** (2.00 $10^{-5}$ M) in dichloromethane.

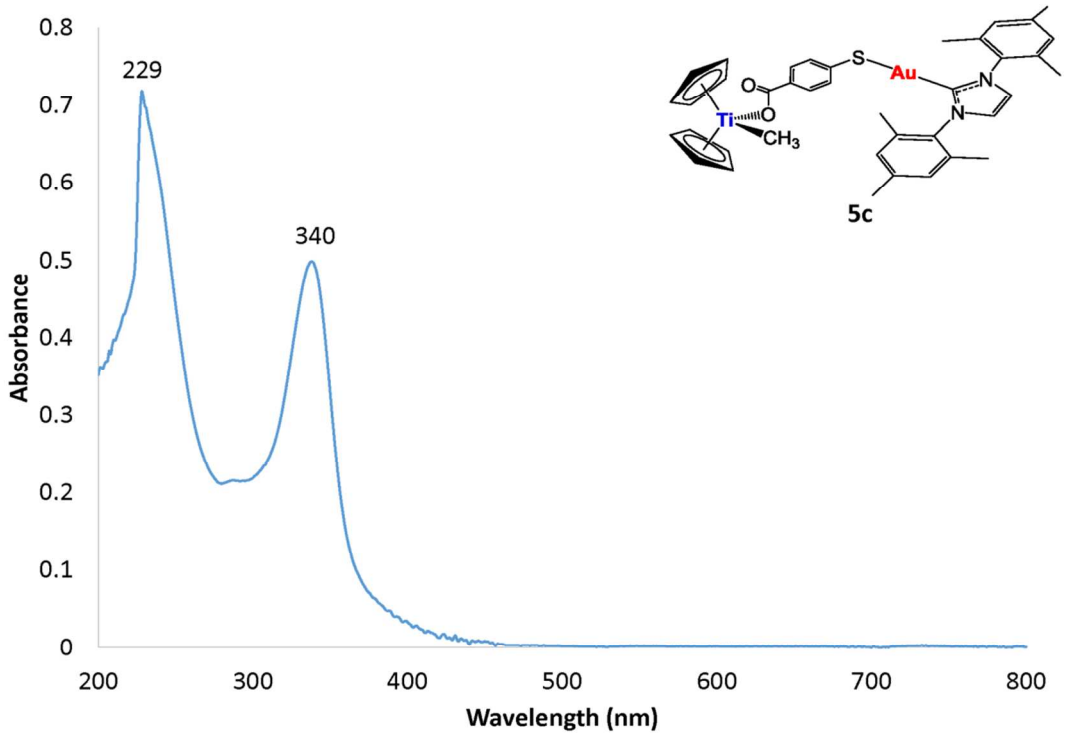


**Figure S47.** UV-visible spectrum of compound **5c** (1.72 $10^{-5}$ M) in dichloromethane.

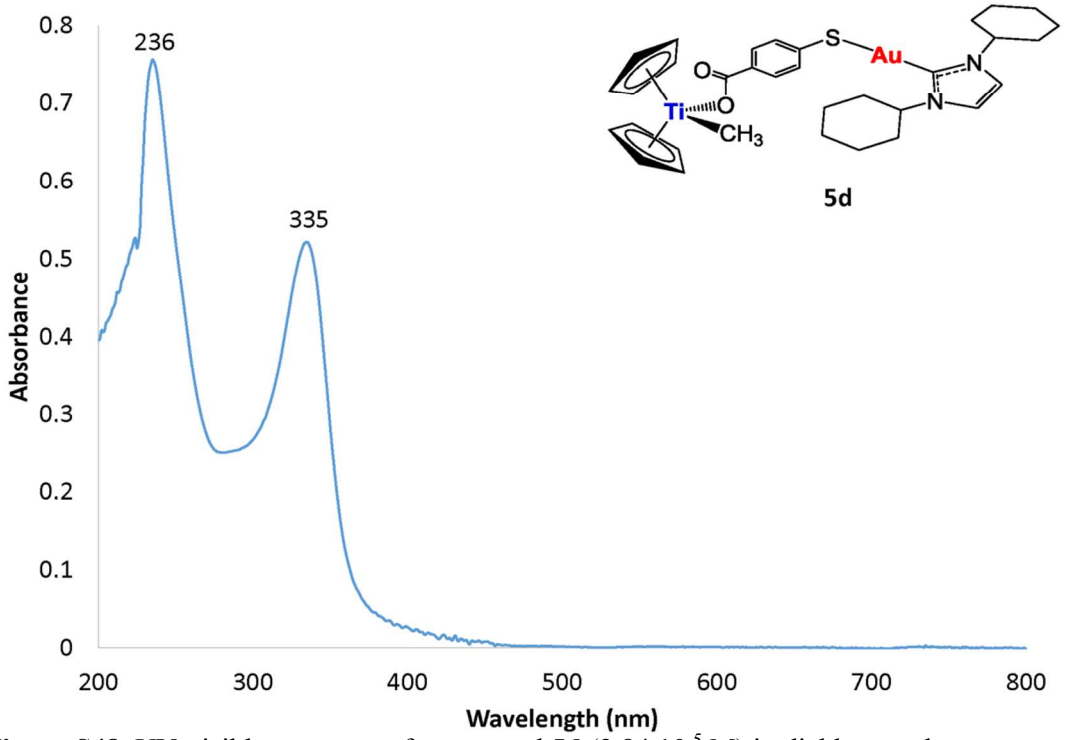


**Figure S48.** UV-visible spectrum of compound **5d** (2.84 $10^{-5}$ M) in dichloromethane.

**6.** Crystallographic data for compound **4c**

**Table S1.** Crystal Data and Structure Refinement for compound **4c**.

| | |
|---|---|
| formula | $C_{28}H_{29}AuN_2O_2S$ |
| fw | 654.56 |
| T [K] | 293 (2) |
| λ ($Mo_{K\alpha}$)[Å] | 0.71073 |
| crystal system | Triclinic |
| space group | P-1 |
| *a* [Å] | 12.093(2) |
| *b* [Å] | 15.270(3) |
| *c* [Å] | 17.367(4) |
| α [°] | 66.62(3) |
| β [°] | 75.42(3) |
| γ [°] | 89.04(3) |
| V [Å]$^3$ | 2836.4(10) |
| Z | 4 |
| $D_{calcd}$ (mg m$^{-3}$) | 1.533 |
| μ (mm$^{-1}$) | 5.285 |
| F(000) | 1288 |
| Crystal size (mm) | 0.24 x 0.22 x 0.21 |
| Theta range for data collection | 1.33 to 27.53 deg. |
| Limiting indices | -15<=h<=15,-19<=k<=19,-22<=l<=22 |
| Reflections collected / unique | 22162 / 12924 [R(int) = 0.0300] |
| Completeness to theta = 24.71 | 98.8 % |
| Refinement method | Full-matrix least-squares on $F^2$ |
| Data / restraints / parameters | 12924 / 0 / 613 |
| GOF | 0.785 |
| Final R indices [I>2$\sigma$(I)] | R1 = 0.0359, wR2 = 0.0869 |
| R indices (all data) | R1 = 0.0636, wR2 = 0.0991 |
| Largest diff. peak and hole | 1.220 and -1.151 e.A$^{-3}$ |

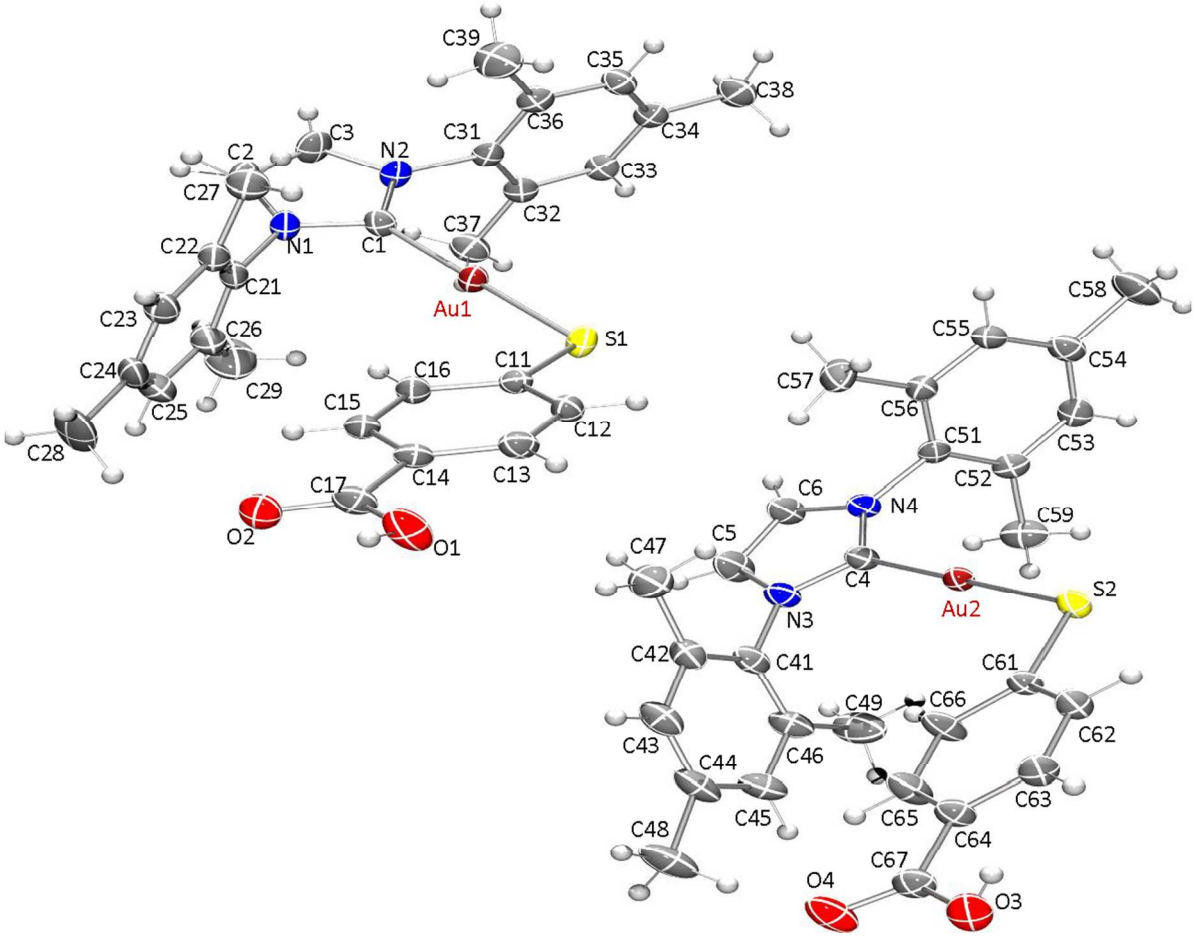


**Figure S49**. ORTEP view of the molecular structure of compound **4c** showing labelling scheme.

**Table S2**. Selected Structural Parameters of compound **4c** from X-ray single crystal diffraction studies. Bond lengths in Å and angles in °.

| | | | |
|---|---|---|---|
| Au(1)-C(1) | 1.995(6) | C(1)-Au(1)-S(1) | 177.76(18) |
| Au(1)-S(1) | 2.2790(17) | C(11)-S(1)-Au(1) | 105.92(19) |
| S(1)-C(11) | 1.746(6) | C(1)-N(1)-C(2) | 111.4(5) |
| C(1)-N(1) | 1.353(7) | C(1)-N(1)-C(21) | 123.4(5) |
| C(1)-N(2) | 1.341(7) | C(2)-N(1)-C(21) | 125.2(5) |
| N(1)-C(2) | 1.381(8) | N(2)-C(1)-N(1) | 104.2(5) |
| N(1)-C(21) | 1.453(7) | N(2)-C(1)-Au(1) | 129.8(4) |
| N(2)-C(3) | 1.382(7) | N(1)-C(1)-Au(1) | 126.0(4) |
| N(2)-C(31) | 1.456(7) | C(1)-N(2)-C(3) | 111.1(5) |
| C(2)-C(3) | 1.335(9) | C(1)-N(2)-C(31) | 124.8(4) |
| O(1)-C(17) | 1.288(8) | C(3)-N(2)-C(31) | 124.1(5) |
| O(2)-C(17) | 1.240(8) | C(3)-C(2)-N(1) | 106.2(5) |
| Au(2)-C(4) | 1.994(6) | C(4)-Au(2)-S(2) | 179.03(17) |
| Au(2)-S(2) | 2.2888(17) | C(61)-S(2)-Au(2) | 105.90(18) |
| S(2)-C(61) | 1.753(5) | C(4)-N(3)-C(5) | 110.7(5) |
| C(4)-N(3) | 1.348(7) | C(4)-N(3)-C(41) | 124.4(5) |
| C(4)-N(4) | 1.357(7) | C(5)-N(3)-C(41) | 124.9(5) |
| N(3)-C(5) | 1.387(8) | N(3)-C(4)-N(4) | 105.2(5) |
| N(3)-C(41) | 1.440(7) | N(3)-C(4)-Au(2) | 125.9(4) |
| N(4)-C(6) | 1.385(7) | N(4)-C(4)-Au(2) | 128.8(4) |
| N(4)-C(51) | 1.440(7) | C(4)-N(4)-C(6) | 110.7(5) |
| C(5)-C(6) | 1.352(9) | C(4)-N(4)-C(51) | 125.8(4) |
| O(3)-C(67) | 1.289(8) | C(6)-N(4)-C(51) | 123.4(5) |
| O(4)-C(67) | 1.239(8) | C(5)-C(6)-N(4) | 106.5(5) |

## 7. DFT Studies for compounds **4a-d** and **5a-d**

7.1. Computational details and structures.

The calculations have been performed using the hybrid density functional method B3LYP,[4] as implemented in Gaussian09.[5] Geometries were optimized with the 6-311G(d) basis set for the P and S elements, the 6-31G(d,p) basis set for the C, N, S, and H elements and the SDD pseudopotential for the titanium, iron and gold metal centers.[6] Frequency calculations have been done at the same level of theory as the geometry optimizations to confirm the nature of the stationary points.

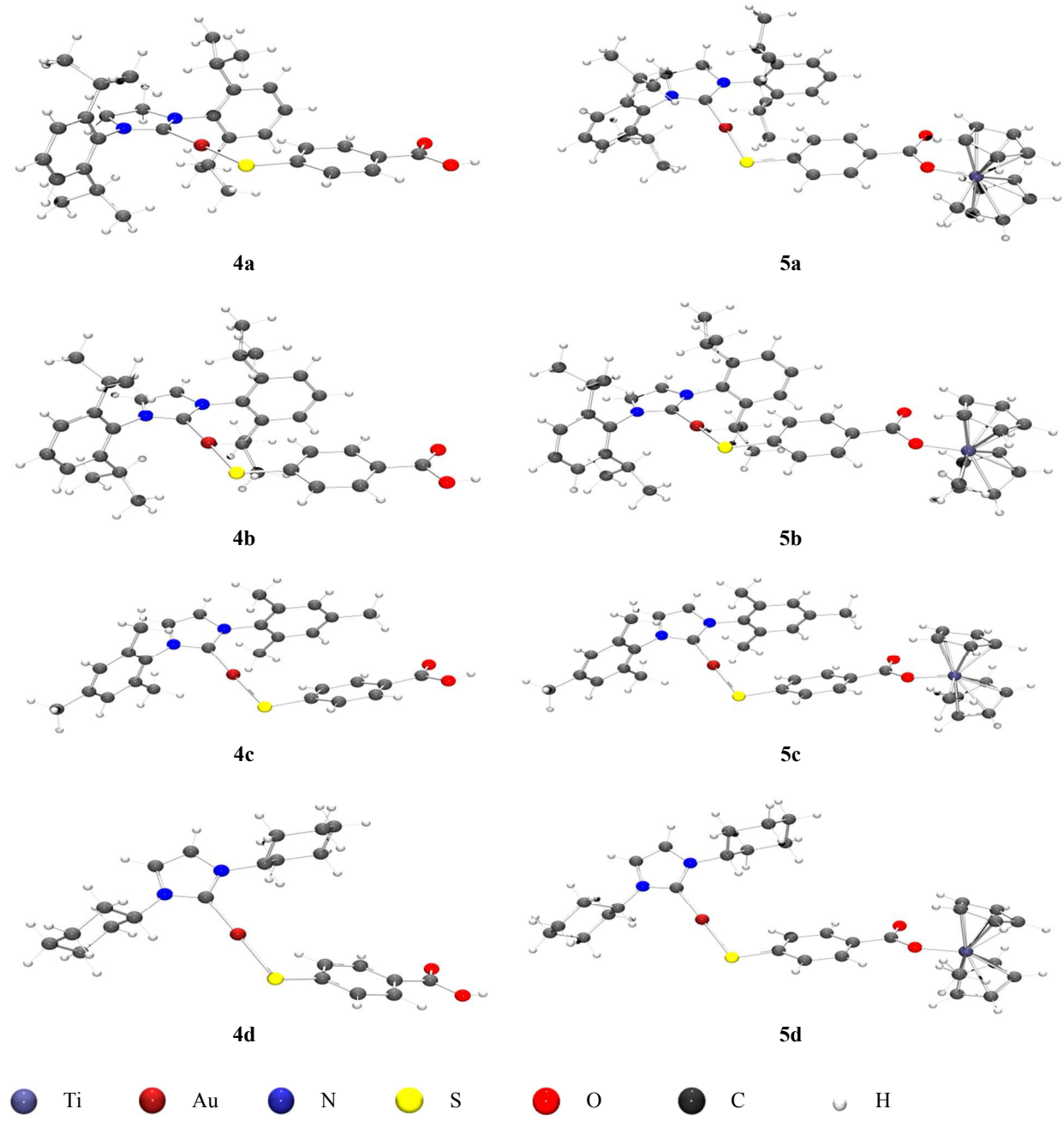


**Figure S50**. Optimized structures of monometallic compounds **4a-d** and bimetallic compounds **5a-d**.

7.2. Calculated IR spectra of compounds **4a-d** and **5a-d**

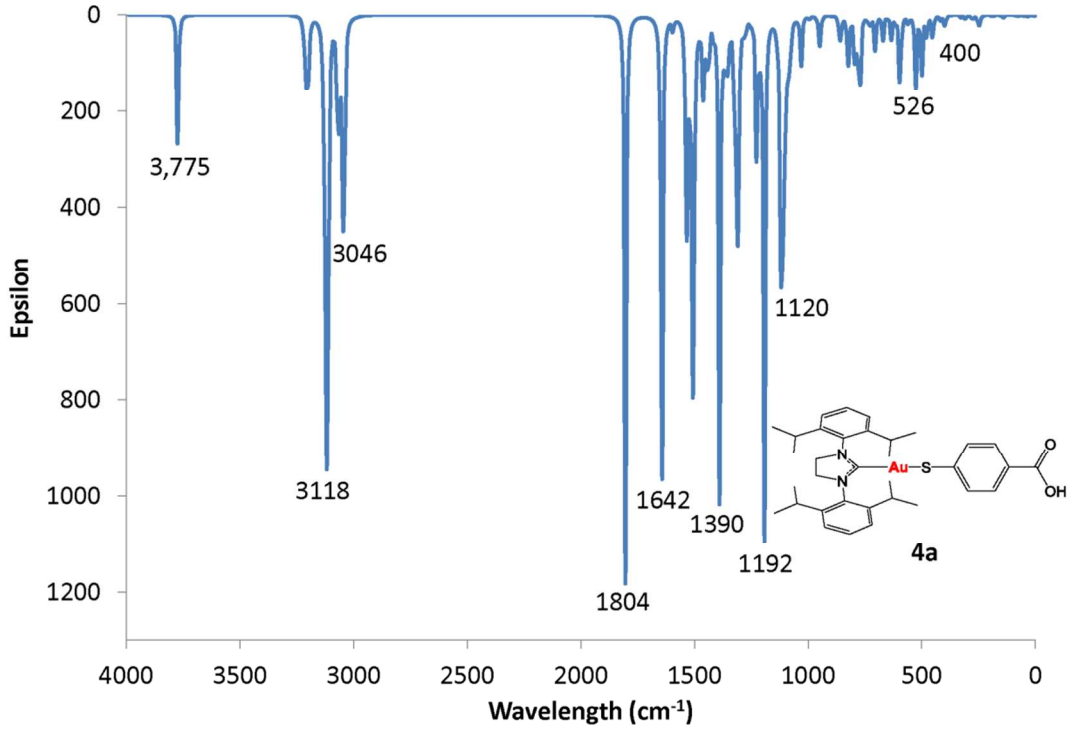


**Figure S51**.Calculated IR spectrum of compound **4a**.

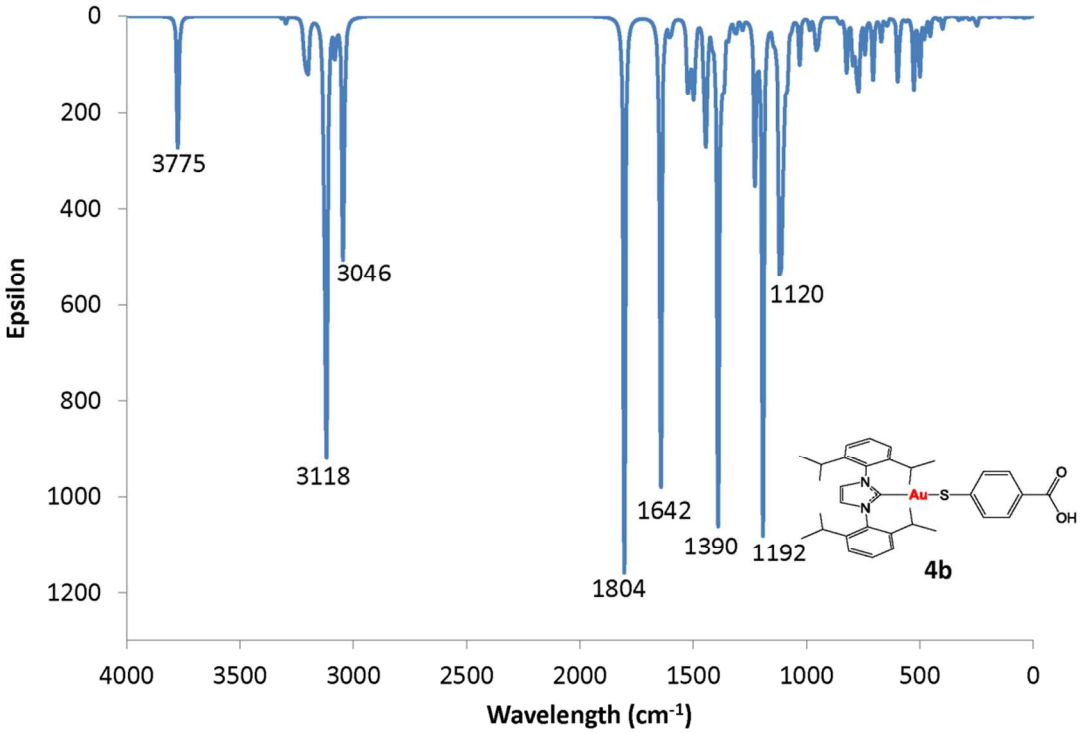


**Figure S52**.Calculated IR spectrum of compound **4b**.

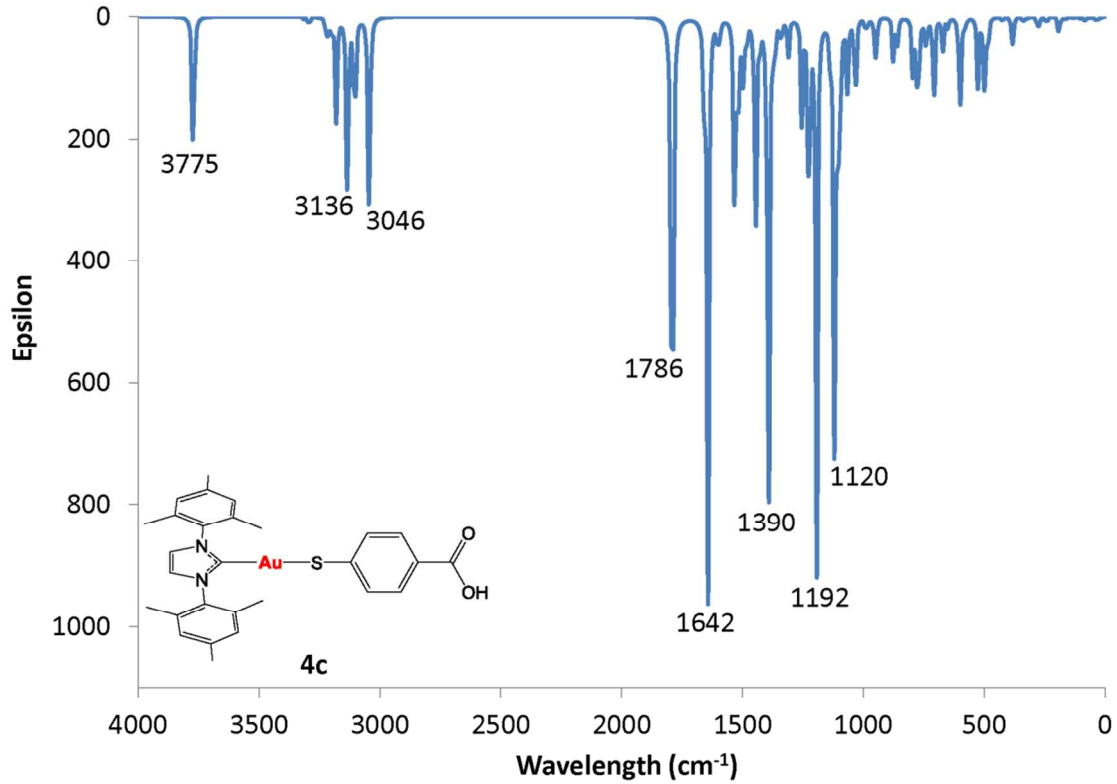


**Figure S53**.Calculated IR spectrum of compound **4c**.

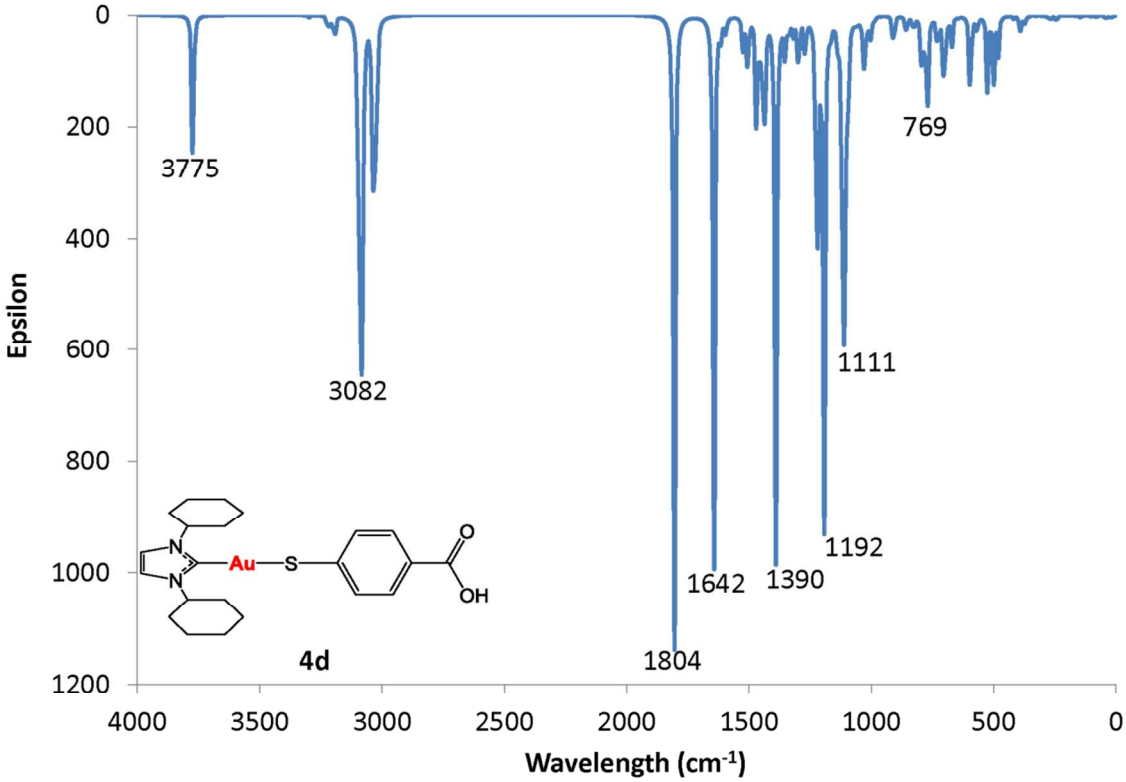


**Figure S54**.Calculated IR spectrum of compound **4d**.

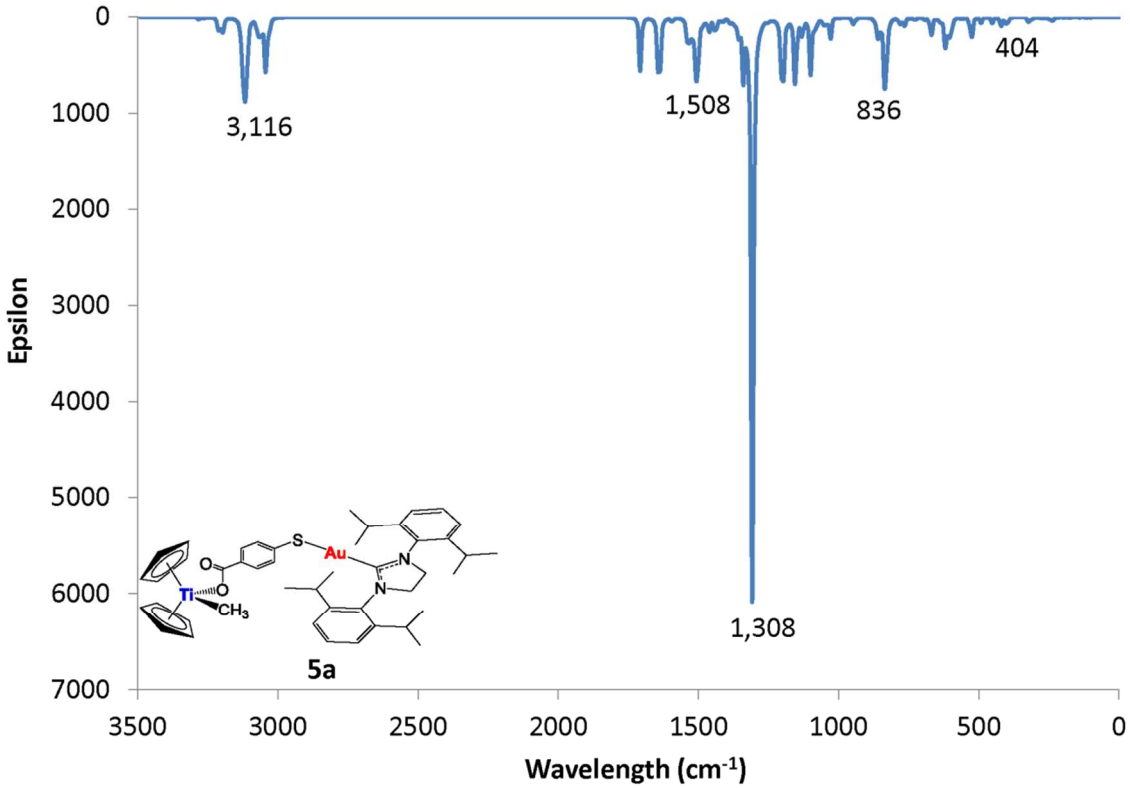


**Figure S55**.Calculated IR spectrum of compound **5a**.

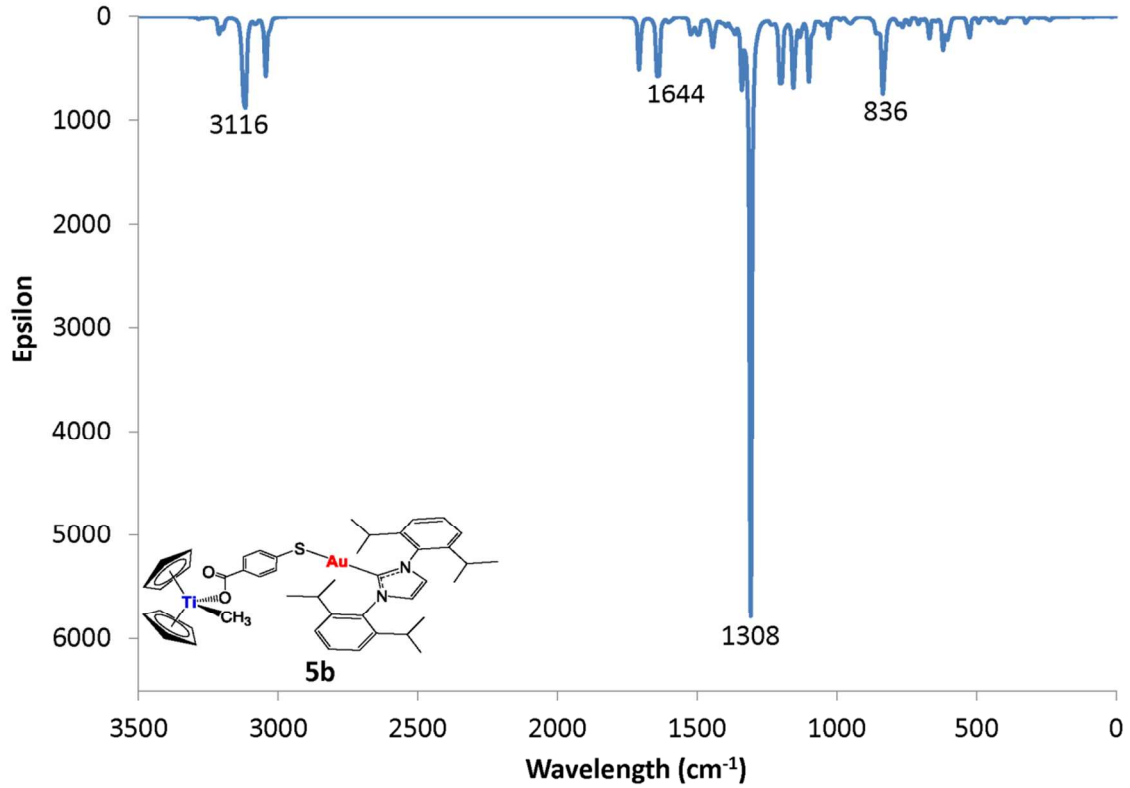


**Figure S56**.Calculated IR spectrum of compound **5b**.

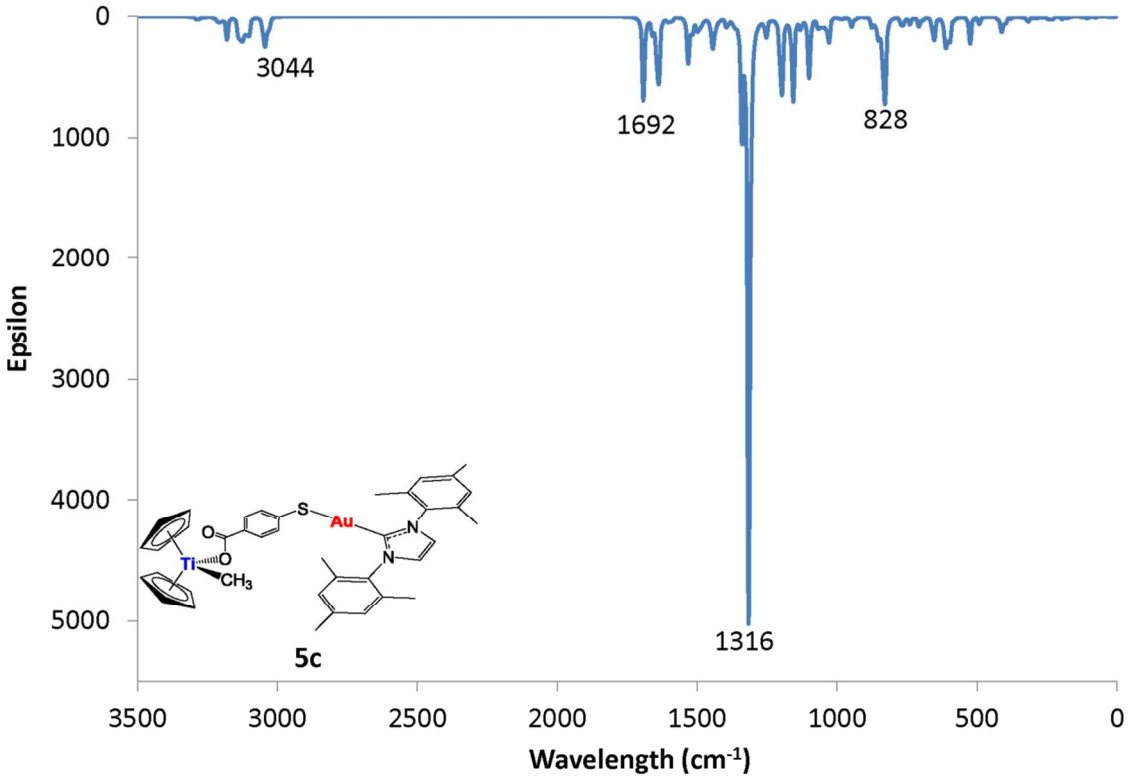


**Figure S57**.Calculated IR spectrum of compound **5c**.

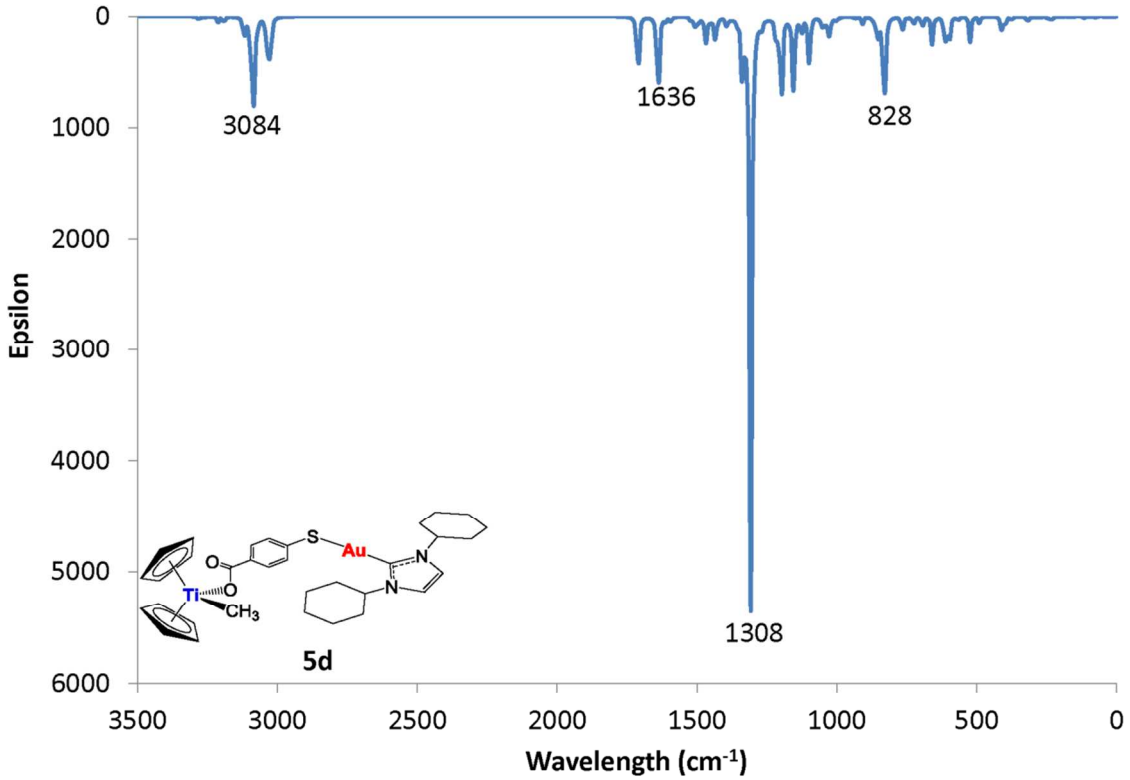


**Figure S58**.Calculated IR spectrum of compound **5d**.

**8.** Interaction of monometallic gold compounds (**4a-d**) with plasmid pBR322 DNA

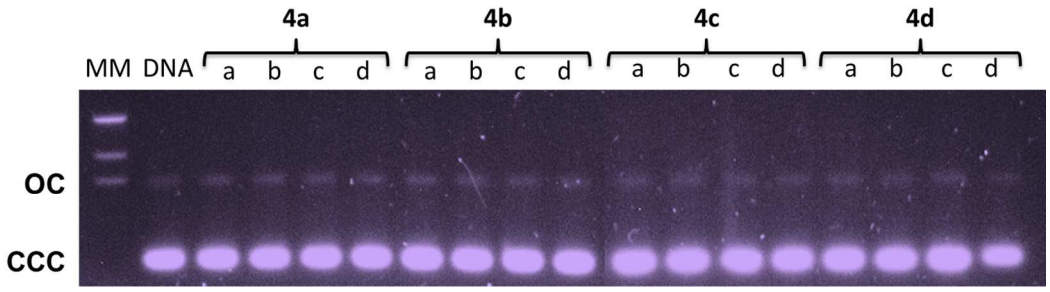


**Figure S59**. Electrophoresis mobility shift assays for monometallic Au compounds **4a-d** (see Experimental for details). DNA refers to untreated plasmid pBR322. a, b, c and d correspond to metal/DNA bp ratios of 0.25, 0.5, 1.0 and 2.0 respectively.

**9.** Migration assays with compounds **4a** and **4c**

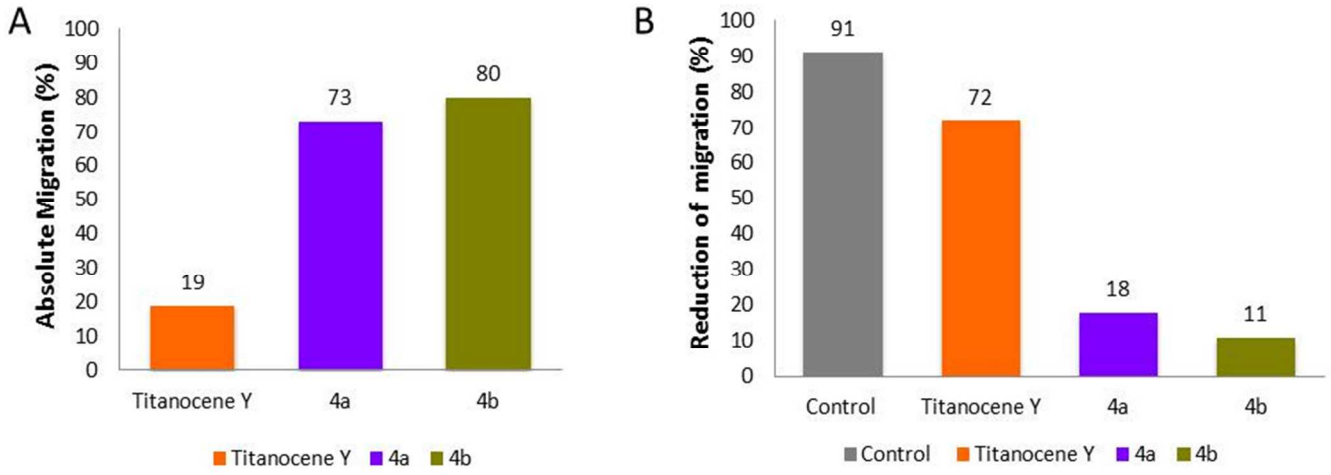


**Figure S60**. Cell migration in **4a** or **4b** treated PC3 cells. Migration of PC3 cells was assessed using a wound-healing assay following treatment with 15 $\mu$M Titanocene Y, 15 $\mu$M of **4a** or **4b** incubated for 24 hours (values normalized against 0.1% DMSO control). **A**. Absolute migration (%). **B**. Reduction of migration (%).

**10.** Inhibition of Thioredoxin Reductase (TrxR) studies of Titanocene Y at 5 and 24h

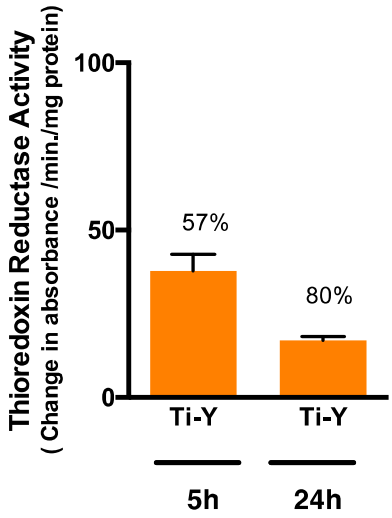


**Figure S61**. Thioredoxin reductase activity in Titanocene Y (Ti-Y) treated PC3 cells. Activity of endogenous PC3 thioredoxin reductase from soluble whole cell lysates following incubation with 15 μM of Titanocene Y for 5 hours, and 24 hours (values normalized against 0.1% DMSO control).